Aeolian Research 55 (2022) 100785

Contents lists available at ScienceDirect

Aeolian Research

journal homepage: www.elsevier.com/locate/aeolia

Grain size analysis of the latest Quaternary Kordofan Sand of Central Sudan: Depositional environment and mode of transportation

Ahmed Dawelbeit [a,*], Etienne Jaillard [b], Ali Eisawi [c]

[a] Department of Geology, Faculty of Science, University of Kordofan, El Obeid, Sudan
[b] Université Grenoble Alpes, ISTerre, IRD-CNRS-IFSTTAR-USMB, CS 40700 38058 Grenoble cedex 9, France
[c] Faculty of Petroleum and Minerals, Al-Neelain University, Khartoum, Sudan

ARTICLE INFO

Keywords:
Holocene
Grain size analysis
Aeolian environment
Saltation population
Energy of transportation
Central Sudan

ABSTRACT

Grain size analysis is a powerful tool for determining the depositional environment. Grain size analysis for 48 samples from four sections along a 280 km long, nearly north–south-trending transect, has been conducted in the mainly Holocene Kordofan Sand in the Kordofan Region of Central Sudan. In these sections, this part of the Kordofan Sand comprises three pedosedimentary sequences. The lower sequence (~13–10 kyr) has been pedogenized during the African Humid Period and ends up farther West with lacustrine or palustrine carbonates. The middle sequence (~6–3 kyr) is represented by sand with low degree of pedogenesis and corresponds to the African Humid Period. The upper sequence was deposited after a hiatus lasting from ~3.3 to 1.1 ka BP, and constitutes the present-day surficial deposits, showing little or no pedogenesis. Spatial grain size distribution and mode of transport show a southward fining trend, indicating that the sandy sediments were transported from north to south. This interpretation is supported by the results of mean grain size – sorting, and sorting – skewness interrelations, which provided a linear relationship. Vertical variation in grain size distribution in the studied sections shows variable energy over time in the north and constant, low energy in the south. The dominance of saltation as a transport mode confirms that the studied sediments were deposited in aeolian environment. The low sorting degree, the presence of coarse grains, and the still active transverse dunes and barchans in the North, indicate that the Late Pleistocene part of the Kordofan Sandstone is submitted to reworking until now. Consequently, the mainly Holocene sand sequences were fed both by distal, fine-grained Saharan material and by proximal, coarser-grained sand proceeding from the Late Pleistocene aeolian dunes.

Introduction

Grain size analysis is a powerful tool for understanding the dynamics and depositional mechanism, transport mode and sorting of sediment particles. Therefore, it is crucial for determining the depositional environments of clastic sediments (e.g. Folk and Ward, 1957; Visher, 1969; Folk, 1971; McLaren and Bowles, 1985; Rajganapathi et al., 2013; Vandenberghe, 2013; Liu et al., 2014; Zhu and Yu, 2014; Vandenberghe et al., 2018). Across the Sahara, several studies aimed at reconstructing the play and variations of aeolian activity through time (e.g. Bakhit and Ibrahim, 1982; Swezey, 2001; Gatto and Zerboni, 2015). Zielhofer et al. (2017) studied the Saharan dust input for the last 12 kyr in the Moroccan Atlas based on multiproxy analysis including grain size. However, no studies used the grain size analysis to assess the mode of transportation of aeolian sands and the spatial variation of the aeolian energy of transportation in Sudan.

In central Sudan, most of the Kordofan region encompasses the transition between Sahara and Sahel. It is covered by what is referred to as the Kordofan Sand (Edmond, 1942; Rodis et al., 1968) and "Qôz" by Whiteman (1971). It consists of unconsolidated surface sands covering large areas to the west of the White Nile (Edmond, 1942), and was considered part of a large zone characterized by widespread dune fields, which extends from about latitude 10° N in the South up to the Sudan-Egypt border in the North (Abdu, 1976). The thickness of this deposit varies from a few inches to up to 200 feet in the dune-like features (Edmond, 1942). Grabham (1935) assumed that the Kordofan Sand was transported by wind from desert areas floored by granitic basement rocks, while Andrew (1948) assumed their local origin. Edmond (1942) suggested that the sand was formed by weathering and reworking of older sandstones (Bakhit and Ibrahim, 1982). Rodis et al. (1968)

* Corresponding author.
E-mail addresses: Ahmeddawelbeit69@gmail.com (A. Dawelbeit), Etienne.Jaillard@Univ-Grenoble-Alpes.fr (E. Jaillard), a.eisawi@neelain.edu.sd (A. Eisawi).

https://doi.org/10.1016/j.aeolia.2022.100785
Received 11 April 2021; Received in revised form 9 February 2022; Accepted 22 February 2022

believed that their reddish color and their gently undulating surface reflect an aeolian origin. However, most of these interpretations are based on geomorphological evidence and field observations. Our recent study showed that the uppermost part of the Kordofan Sand is younger than ≈15 ka BP. Nevertheless, it may be as thick as 7 m and the aeolian sand that encompasses the last 1000 yr is locally more than 2 m-thick (Dawelbeit et al., 2019a). These high sedimentation rates raise the issue of the origin and processes of deposition of the Kordofan Sand. Therefore, the aims of the present study are to determine the transport and deposition processes, and to define the direction and energy of transportation of the Kordofan Sand based on grain size variations through time and space.

Morphology and geology of the Kordofan region

Physiography

The Kordofan region is located in central-southern Sudan (9° – 17° N; 27° – 32.4° E), on the southern border of eastern Sahara (Fig. 1). It is characterized by heterogeneous topography. In its northern part, low-lying, gently undulating topography dominates (Fig. 2A), with few scattered, low-elevated inselbergs mostly composed of magmatic rocks of Paleozoic/Mesozoic age (Abdel Galil, 2008), and isolated outcrops of Mesozoic sandstones. As a whole, this northern part is a gently northward dipping slope (Fig. 2C). It is covered by extensive sand sheets, and North-South oriented linear sand dunes that decrease in size and length southward (Fig. 2B). As the dune field decreases in size, the inter-dune depressions also decrease in size towards the south (Dawelbeit, 2018; Fig. 2). The northern part of the region shows a poor drainage system due to the arid climate and the development of the North-South trending sand dunes that form dams as they cut ancient rivers (Fig. 2B). Therefore, ephemeral rivers may form seasonal lakes behind the sand dunes, or vanish rapidly due to the infiltration of flowing water into the sand dunes (Dawelbeit, 2018).

The southern part of the region shows steep massifs and inselbergs of the "Nuba Mountains", composed of Cambrian igneous rocks (Abdel Galil, 2008). Some of these peaks are up to 1400 m above sea level (Jebel Ed Dair, Fig. 2A). The plains consist of dark grey soils locally interspersed with some sands and sand dunes further north (Dawelbeit, 2018). Because of a more humid climate, this area is characterized by deep V-shaped valleys and saddles. The southern part is dominated by a channelized, meandering, well-developed drainage pattern due to more abundant rainfall. Small streams form the tributaries of Khour Abu Habil, or flow southward to the Sudd area, and then to the White Nile River.

The central part of the region is an elevated area, and separates these two areas. West of the central part of the study area, a plateau forms the En Nahud-El Khowei groundwater basin. This plateau consists of Mesozoic sandstones and is controlled by NNW-SSE- and E-W-trending fault systems (Elmansour and Omer, 2017). There, the relief is dominated by smooth V-shaped valleys, while to the east and around Khour Abu Habil, the relief is dominated by broad wadis (Dawelbeit, 2018). The abundance of sand dunes and sheets in the central part of the region results in a coarse dendritic drainage system (Elmansour, 2017) with intense infiltration. The surface water of this area is drained to the south (Fig. 2).

Pre-quaternary sediments

The study area includes a highly discontinuous rock record ranging from Precambrian to Recent time (Rodis et al., 1968; Whiteman, 1971; Vail, 1978). Precambrian rocks include high- to low-grade metamorphic rocks, intruded by late- to post-orogenic granites, and acid volcanic rocks. These are locally overlain by sandstone, shale, and thin limestone

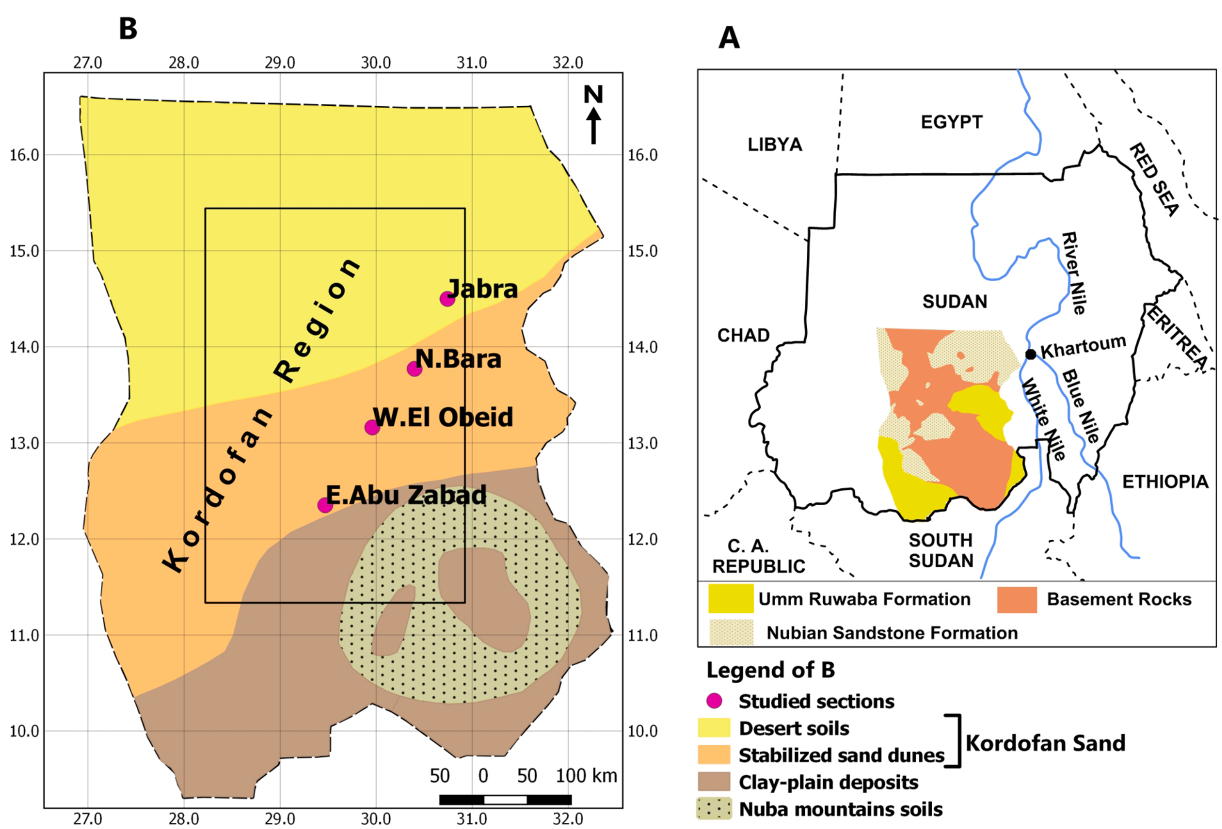

Fig. 1. Location map of the study area. A: location of the Kordofan Region and the general distribution geological units in the Region. B: general distribution of surficial deposits in the Kordofan Region (in Rodis et al., 1968). The block on B is the study area, shown in detail in Fig. 2.

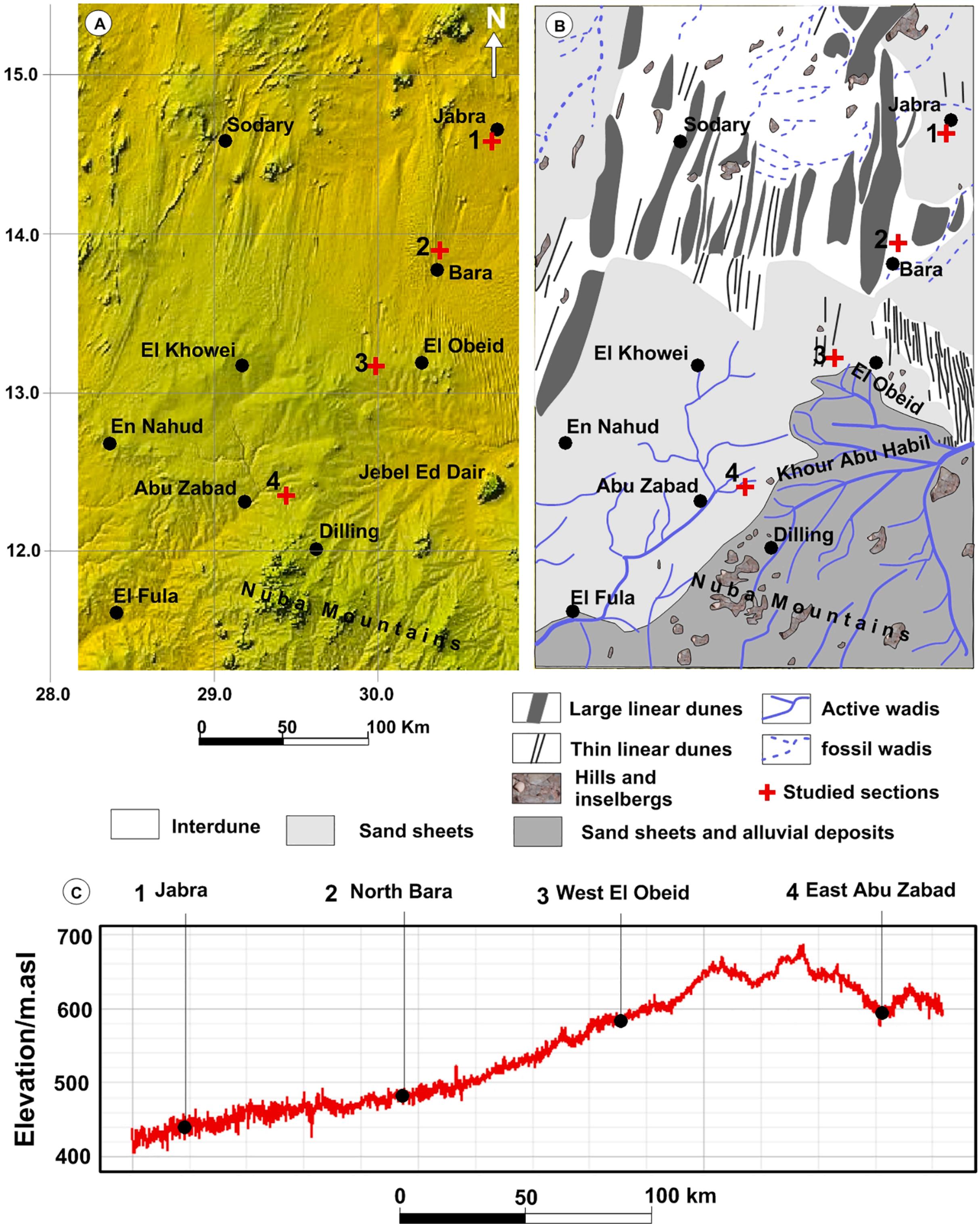

Fig. 2. Physiography of the study area. A: hill-shade image showing the relief of the study area; B: geomorphological features appearing in A. C: Northeast-Southwest topographic profile showing the topographic gradient in the study area. The studied sections are located by black points on the profile.

beds attributed to the Paleozoic-Mesozoic. The widespread Nubian Group consists of conglomerates, sandstone, and mudstone, deposited in continental to nearshore environments and assigned to the Cretaceous (McKee, 1963; Schrank, 1994). They contain abundant iron-rich concretions, which are assumed to have formed before mid-Miocene times (Schwarz, 1994) and are frequently reworked in fluvial deposits in the southern part of the studied area (Dawelbeit, 2018). The Nubian Group is overlain by the Umm Ruwaba Formation, which is restricted to the southeastern and eastern parts of the study area (fig. 1a). It consists mostly of mudstone, sandstone, and conglomerates of lacustrine and fluvial environments attributed to the late Miocene to Pleistocene (el shafie et al., 2013).

Stratigraphy of the Kordofan Sand

The Quaternary Kordofan Sand is composed of fine- to medium-grained sand (Ginaya, 2011) and is believed to represent the southernmost windblown sand of the Sahara (Elmansour, 2017). It is characteristically made of well-rounded quartz grains (Edmond, 1942) and its colour varies from pale buff to deep red (Edmond, 1942; Rodis et al., 1968; Dawelbeit et al., 2019a) and is considered latest Pleistocene to Holocene in age (Dawelbeit et al., 2019a). The red colour is due to iron staining of the surface of the grains (Edmond, 1942). These partially stabilized sand dunes and sand sheets grade northward into coarse residual soils and active sand dunes (Rodis et al., 1968), which may have formed during the Last Glacial Maximum (≈20–15 ka BP). The latter period was marked by quite arid conditions (Williams et al., 2006; Gasse et al., 2008) and a strong aeolian activity (Nicholson and Flohn, 1980; Swezey, 2001; Williams, 2009, 2014). The linear dunes crosscut fossil rivers that may have formed during the last interglacial episode (≈130–115 ka BP; Gierz et al., 2017), considered a rainy period (Revel et al., 2010; Tierney et al., 2017). In the central part of the study area, the linear dunes grade southward into sand sheets, upon which subsequent, small scale transverse dunes are superimposed (Whiteman, 1971; Fig. 2A). To the South, the Kordofan Sand inter-fingers with clay-plain deposits (Ruxton and Berry, 1978; Fig. 2). Alluvial deposits in the channels of wadis, khours and slope-wash deposits occur mainly in the southern part of the region; because of their limited aerial extent, they are not shown in Fig. 2.

The stabilized sand structures (Qôz, Whiteman, 1971) are blanketed by fine-grained sand that form the present-day soil and surficial ground water reservoir in the Kordofan region. The stratigraphy of the latter has been recently revised, using numerous sedimentary sections and ^{14}C dating, and is now dated as mainly Holocene in age (Dawelbeit et al., 2019a; 2019b; Fig. 3). The thickness of the studied sections reaches 720 cm. Climate is thought to be the main factor controlling the temporal and spatial distribution of these deposits (Dawelbeit et al., 2019a). Between ~13 kyr and ~10.5 kyr BP, an arid climate prevailed in the Kordofan region, except in the southern areas. This arid climate led to the deposition of sand interpreted as aeolian sediment in most parts of the region (U 1 on Fig. 3). Then, the region was subjected to the well-known "African Humid Period" (AHP) up to ~6.5 kyr. This period is marked by isolated lacustrine carbonates in the North, by abundant palustrine and lacustrine carbonates dated between 10.5 and 6.5 kyr to the West (Williams, 2009; Dawelbeit et al., 2019a), by fluvial deposits in the South (U 2, Fig. 3), and by the pedogenesis of earlier deposits throughout the region. During the period from ~6.5 kyr BP up to the present, the climate evolved to arid conditions (U 3, Fig. 3). These are marked by a strong aeolian activity and erosion that peaked between 3.3 and 1.1 kyr BP. Subsequently, aeolian sedimentation resumed and continued until now (U 4, Fig. 3). This evolution is consistent with the aeolian activity documented during the late Pleistocene-Holocene in Central and Eastern Sahara, the Nile Basin and East Africa (Nicholson and Flohn, 1980; Woodward et al., 2007; Tierney et al., 2011; Williams et al., 2000; Williams, 2014; McGee et al., 2013; Egerer et al., 2017). There, Late Quaternary sediments indicate widespread aeolian sediment mobilization prior to 11 kyr BP, aeolian sediment stabilization from 11 to 5 kyr BP, and a return to widespread aeolian sediment mobilization after 5 kyr BP (Swezey, 2001).

In the studied sections, the Kordofan Sand can be divided into three sequences (Fig. 4). The lower sequence consists of sand deposits older than 10.5 kyr BP, which are frequently rich in calcitic nodules (Unit 1 and 2, Fig. 3). This sequence varies in color from grey to pale yellow, and consists of mottled sand. Since mottling and root marks decrease downward, pedogenesis is thought to have occurred during the subsequent AHP. As a matter of fact, in the central part of the study area, the top of this sequence includes the palustrine carbonates mentioned above. This unit corresponds to a pedostratigraphic, or pedosedimentary, sequence as defined by Costantini (2018; Costantini and Priori, 2007) and Zerboni et al. (2015). The maximum measured thickness of this sequence is ≈350 cm. Where visible, the base of the lower sequence unconformably overlies the Cretaceous Nubian Sandstone or the crystalline basement rocks (Dawelbeit, 2018).

The middle sequence consists of pale yellow to light brown, slightly mottled and weathered sand dated between 4.5 and 3 kyr (Dawelbeit et al., 2019a; Fig. 3). This unit is virtually free of calcitic nodules. It corresponds to the period of aridification that followed the AHP and has been removed by the subsequent aeolian erosion in large areas of the central and northern parts of the studied region. The thickness of this sequence reaches about 350 cm. Since it is followed by a sedimentary hiatus, it is interpreted as a new pedosedimentary sequence.

The upper sequence corresponds to the aeolian sediment deposited after 1.1 kyr BP (Unit 4 of Fig. 3). It overlies the middle sequence

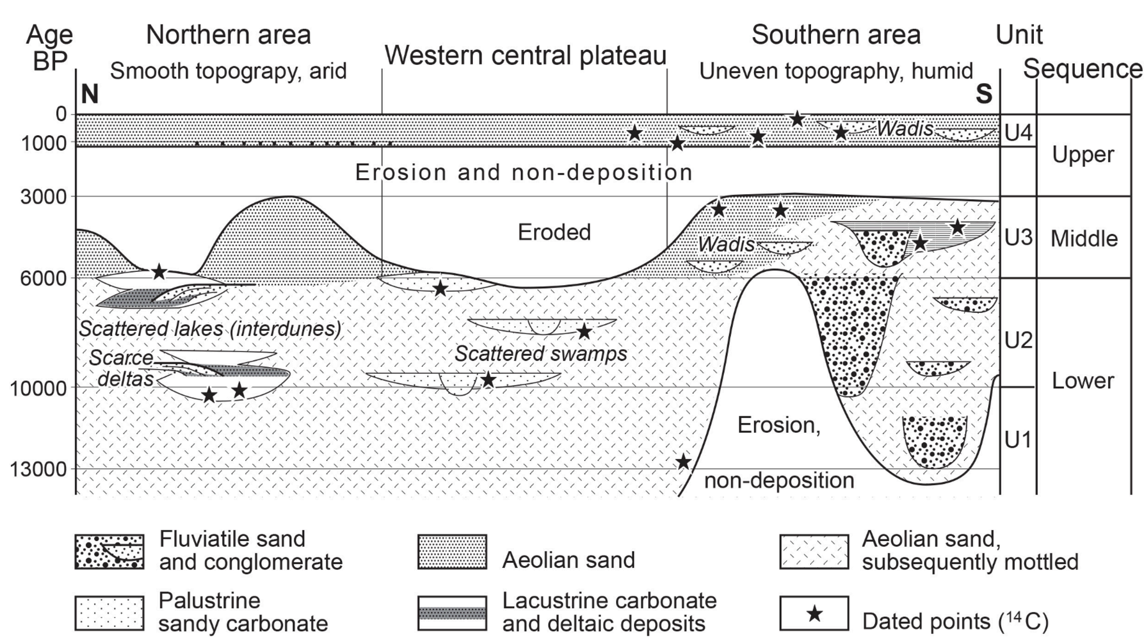

Fig. 3. Synthesis of the latest Pleistocene-Holocene chronostratigraphic and climatic evolution of the Kordofan Region. (based on Dawelbeit et al., 2019a).

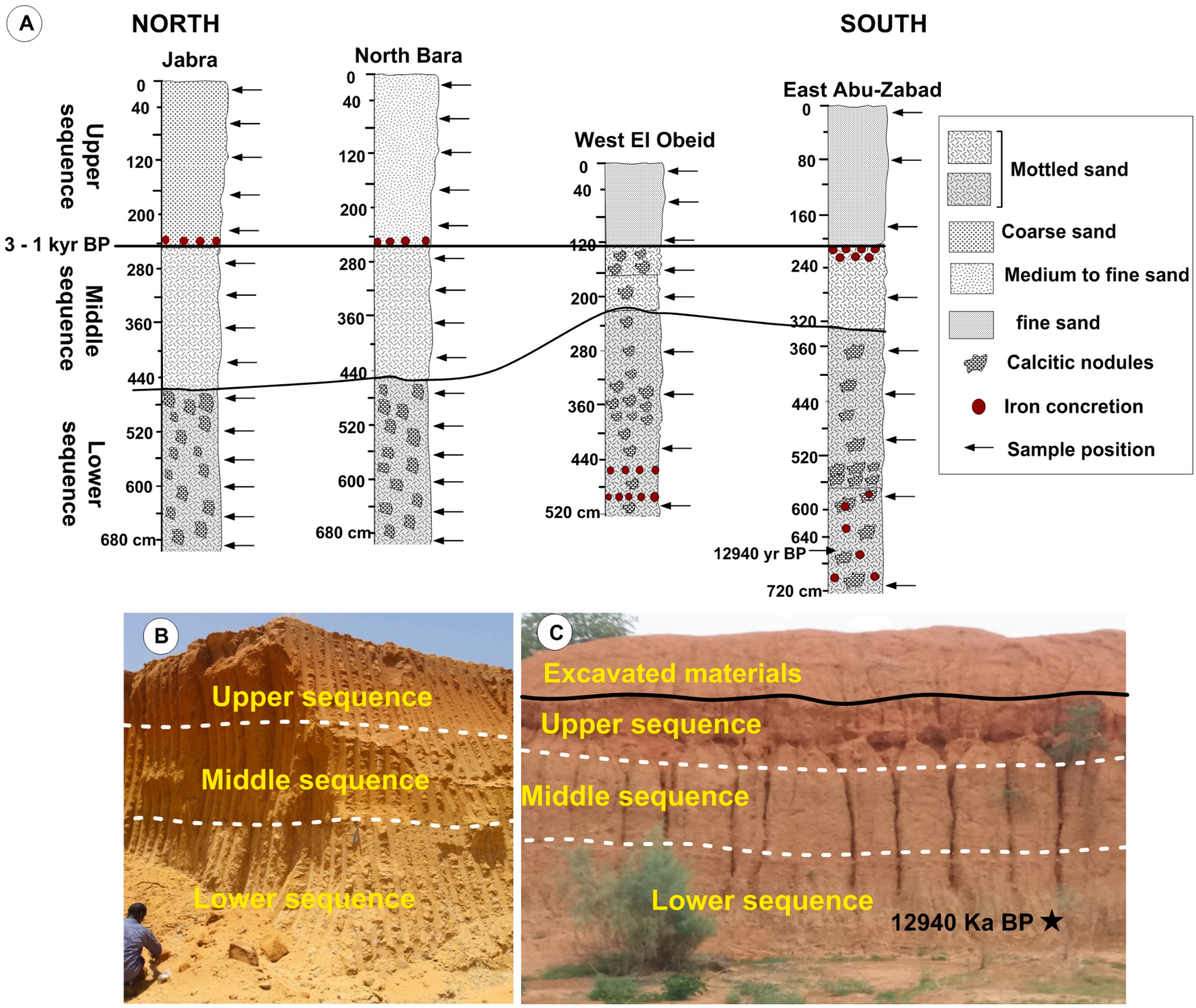

Fig. 4. Pedostratigraphy of the Kordofan Sand. (A) Sequences of the studied sections. (B) and (C): Photographs of the Kordofan Sand from Jabra and East Abu Zabad sections, respectively. Location on Fig. 2.

through an erosional, or a deflation surface (Fig. 4). In the latter case, a thin gravelly layer represents the hiatus occurring between 3.3 and 1.1 ka BP, which is responsible for the erosion of previous deposits (Dawelbeit et al., 2019a). The upper sequence is formed entirely of coarse- to fine-grained red sand in the North and red fine sand in the South. Its maximum measured thickness is ≈ 255 cm. Its uppermost part is locally reworked by human activity (e.g. Fig. 4C), and contains scarce root remnants without evidence of clear pedogenesis in the North. To the South, the upper sequence is locally reworked by fluvial activity (Dawelbeit et al., 2019a); the East Abu Zabad section is preserved of such reworking, and has been, therefore, chosen for this study. Although pedogenesis appears absent, or little developed in the northern and southern sections, we interpret the upper sequence as an upper pedo-sedimentary sequence (Zerboni et al., 2015; Costantini, 2018).

Material and methods

Forty-eight samples from four excavated sections were systematically collected for grain size analysis. The studied sections are: Jabra, North Bara, West El-Obeid, and East Abu-Zabad, which are aligned along a 280 km long, NNE-SSW trending transect (Fig. 1). Bulk samples range in weight from 500 to 800 g, while sieved samples range from 400 to 500 g. All sampled sections include the three sequences.

Since the presence of calcitic nodules and iron concretions in the lower and middle sequences can affect the results of grain size analyses, care was taken during sampling to avoid sampling zones with abundant calcitic nodules, and we completely avoid sampling zones that contain iron concretions. However, in order to avoid these nodules to be considered as individual grains, the calcareous nodules were removed before performing the grain size analysis. The coarse nodules were removed manually in the field, while the smaller ones were treated in the laboratory with sieve meshes larger than the individual grains and smaller than the nodules. In addition, although the analyzed sediments are friable, the preparation steps included the brake up of all staking particles and it was ensured that no cementation was present.

Grain size analysis was carried out at the Department of Geology, University of Kordofan, following standard procedures described by Folk (1971). Samples were dry-sieved in a sieve with an opening range of 2.83 to 0.074 mm for five minutes, using a mechanical shaker. An electronic balance with a sensitivity of 0.1 g was used to weigh the retained material in each sieve. Due to the absence of sieve meshes smaller than 0.074 mm, material smaller than this size was not analyzed, and a single weight percentage is reported and plotted to represent all grains finer than this size. Because cumulative curves have an “S-shape” and we used a minimum mesh size of 0.074 mm, only rough estimates of the silt and clay fraction (material < smaller than 0.063 mm), was obtained by an approximate drawing of the end the curves to represent particles finer than 0.074 mm.

Surfer 11 software was used to plot the cumulative curves of the samples. Statistical grain size parameters (mean grain size, standard deviation or sorting, skewness, and kurtosis) can be used to reflect differences in the sediment characteristics, as well as to refine the depositional environment (Liu et al., 2014). They were calculated for each sample following Folk and Ward (1957; Eqs. (1) to (4)). Mean grain size represents average grain size; sorting (as standard deviation) refers to the uniformity of grain size in the sediment; and skewness measures the asymmetry of the size distribution curve (Folk, 1971).

$$M_Z + \frac{\varnothing_{16} + \varnothing_{50} + \varnothing_{84}}{3} \tag{1}$$

$$\sigma_I = \frac{\varnothing_{84} - \varnothing_{16}}{4} + \frac{\varnothing_{95} - \varnothing_{5}}{6.6} \tag{2}$$

$$SK_I = \frac{\varnothing_{16} + \varnothing_{84} - \varnothing_{50}}{2(\varnothing_{84} - \varnothing_{16})} + \frac{\varnothing_{5} + \varnothing_{95} - \varnothing_{50}}{2(\varnothing_{95} - \varnothing_{5})} \tag{3}$$

$$K_G = \frac{\varnothing_{95} - \varnothing_{5}}{2.44(\varnothing_{75} - \varnothing_{25})} \tag{4}$$

where: $\mathbf{M_Z}$ is the mean size; σ_I is the inclusive graphical standard deviation; $\mathbf{SK_I}$ is the inclusive graphical skewness; $\mathbf{K_G}$ is the graphical kurtosis; and $\mathbf{Ø_n}$ is the diameter, for which n% of the sample is greater than that diameter.

The scales of Udden (1914) and Wentworth (1922) were used to separate the grain size fractions (very fine gravel, very coarse sand, coarse sand, medium sand, fine sand, very fine sand, and mud). Moreover, the percentages of grain size fractions were calculated for each curve by intersecting the limits of each grain size fraction with the representative curve. Since these curves are cumulative, the values obtained for the fraction limits are also cumulative. The normal percentages of each fraction represent the difference between their cumulative limits. Finally, the fractions were plotted in vertical graphs according to the collection depth of the corresponding sample in order to understand their vertical distribution and thus, to illustrate the energy variation of the transport process over time.

Log-probability curves are considered informative with respect to depositional processes and modes of transport. Sediment can be transported by fluids through three basic processes: rolling over the surface (traction), jumping a short distance near the surface (saltation), and suspended in the air (Visher, 1969; Vandenberghe, 2013). Therefore, log-probability curves (Visher, 1969) were constructed to understand the mode(s) of sediment transport in each sample and then in each part of the studied sections. Each mode of transport represents an individual subpopulation within a grain size distribution separated by truncation points (Visher, 1969). However, grains that experienced distinct

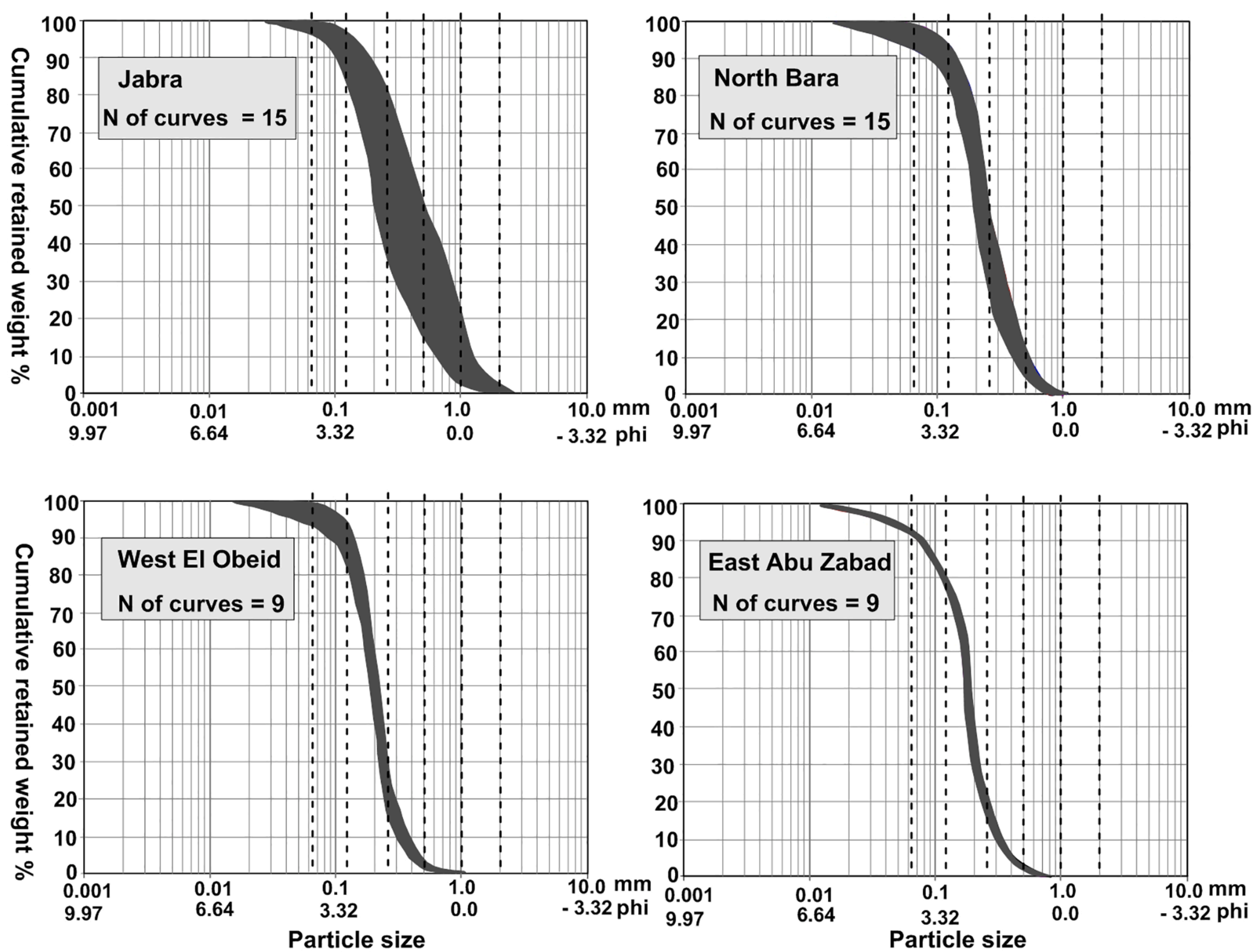

Fig. 5. Cumulative grain size distribution for all samples from the studied sections. The vertical dashed lines are the boundaries between grain size fractions, e.g. from left to right: very fine gravel-very coarse sand, very coarse sand-coarse sand, coarse sand-medium sand, medium sand-fine sand, fine sand-very fine sand, and very fine sand-mud boundaries.

sediment transport mode may be mixed in a same sample (Bagnold, 1941). The log-probability curve usually shows two or three straight line segments, though in some cases four segments may be found (Visher, 1969).

Plotting log-probability curves requires multiple record points of cumulative weight *versus* grain size. However, since we used only one set of six sieves in addition to the pan, we modified the "Visher method" by selecting multiple recording points (intersection points between cumulative weights and grain size) from the previously constructed normal cumulative curves to help constructing the log-probability curves. Since the log probability curve consists of at least three segments, the more plotting points we have, the greater the accuracy.

Results

The grain size distribution of the studied samples is presented in normal cumulative curves and log-probability cumulative curves (Figs. 5 and 8).

Cumulative curves

In semi-logarithmic distribution plot, the cumulative curves of forty-eight samples from the four sections were plotted and compiled into one graph and then displayed in the form of a shaded zone for each section (Fig. 5). The curves are distributed in size range from 2.6 to 0.012 mm (−1.38 and 6.38 Φ). The maximum and minimum grain sizes are recorded in the Jabra and East Abu Zabad sections, respectively (Table 1).

To understand the stratigraphic and geographic evolution of transport processes and energy, the data presented in Table 1 are translated into vertical cumulative grain size plots for each section (Fig. 6). In the Jabra section the grain size percentages show some similarity in percentages of the coarse, medium and fine sand as the dominant sizes along the section. However, fine gravels are scarce and are recorded only in the middle sequence and at the base of the upper sequence (Table 1 and Fig. 6). The very coarse sand has considerable percentage in the upper sequence and around the contact between the middle and upper sequence. In the North Bara section, the grain size percentage is dominated by medium and fine sand in all sequences, while in the West El Obeid and East Abu Zabad sections, the grain size percentage showed an absolute dominance of fine sand in all sequences (Fig. 6).

Mean grain size

The mean grain size (M_Z) values of the studied samples range between 0.57 and 0.17 mm (1.02 and 2.54 Φ). The maximum and minimum grain sizes are recorded in the Jabra and East Abu Zabad sections, respectively. In the Jabra section, 93.3% of the analyzed samples have M_Z that falls in the medium sand range, while 6.7% (one sample at the base of the lower sequence) fall in the medium sand range. In the North Bara section, M_Z values of 86.7% of the samples fall in the fine sand range, while 13.3% (two samples around the contact between the upper and middle sequences) plot in the medium sand range. In the West El Obeid and East Abu Zabad sections, all samples fall in the fine sand range (Table 2; Fig. 7).

Standard deviation

The standard deviation values (σ_I) for all samples range from 0.57 to 1.3 Φ, recorded in West El Obeid and Jabra, respectively. In the Jabra section, 20% of the samples are moderately sorted and 80% are poorly sorted. All standard deviation values at the North Bara section described the samples as moderately sorted. 22% of the samples from the West El Obeid section are moderately sorted (at the base of the lower sequence) and 78% are moderately well sorted. In the East Abu Zabad section all samples are moderately well sorted (Table 2; Fig. 7).

Table 1
Percentages of grain size fractions for the studied samples. Samples are numbered sequentially from top to bottom in each section. VFG = very fine gravel, VCS = very coarse sand, CS = coarse sand, MS = medium sand, FS = fine sand, VFS = very fine sand, Mud = silt and clay fractions.

Section	Sample/ Curve	VFG %	VCS %	CS %	MS %	FS %	VFS %	Mud %
Jabra	Jab 1	–	4	21	26	28	17	4
	Jab 2	–	13	22	20	31	13	1
	Jab 3	–	12	22	17	31	15	3
	Jab 4	–	15	26	25	23.8	9.4	0.8
	Jab 5	1	14	29	23	24	8.3	0.7
	Jab 6	1.8	17.2	31	19	22	8.5	0.5
	Jab 7	1.5	21	27.5	31.5	15	3	0.5
	Jab 8	1.8	9.4	28.8	25	24.5	8.8	1.7
	Jab 9	2	9.5	30	24.5	24	8.2	1.8
	Jab 10	–	10	15	35	25	13.2	1.8
	Jab 11	–	8	15	35	26.5	13.5	2
	Jab 12	–	6.5	15.5	31	32	13	2
	Jab 13	–	7	13.5	26.5	38	13	2
	Jab 14	–	6	12	24	45	11.2	1.8
	Jab15	–	5	11	24	44	14.2	1.8
North Bara	NB 1	–	1	6	50	35.8	8	1.8
	NB 2	–	–	2.5	38.5	46	10	3
	NB 3	–	–	4.5	35.5	46.6	10.4	3
	NB 4	–	–	4.4	36.6	46.8	10.2	2
	NB 5	–	–	4	33.3	52.7	9	1
	NB 6	–	–	4	30	47.2	17	1.8
	NB 7	–	–	6	25	56	11	2
	NB 8	–	–	7	50	26	15.8	1.2
	NB 9	–	–	7	50	26	16.2	0.8
	NB 10	–	–	6.7	45.3	30	15.5	2.5
	NB 11	–	1	3	36	41.5	12.5	6
	NB 12	–	2.8	3.2	30	49	12.7	2.3
	NB 13	–	1	3	31	48	14	3
	NB 14	–	3	4	33	46	11.5	2.5
	NB 15	–	3	5	39	39	12.4	1.6
West El-Obeid	WEO 1	–	–	3	24	56	15	2
	WEO 2	–	–	3	27	55	13.5	1.5
	WEO 3	–	–	3	27	55	13	2
	WEO 4	–	–	3	17	60	18	2
	WEO 5	–	–	2	18	60	17.2	2.8
	WEO 6	–	–	2	18	60	17	3
	WEO 7	–	–	2.8	20.2	60	14	3
	WEO 8	–	–	2	27	51	16	4
	WEO 9	–	1	1.5	17.5	59	16	5
East Abu-Zabad	EAZ 1	–	–	4	22	51	17	6
	EAZ 2	–	–	4	23	52	17	5
	EAZ 3	–	–	4	22	51	17	7
	EAZ 4	–	–	4	14	58	17	7
	EAZ 5	–	–	3	16	56	19	6
	EAZ 6	–	–	3	16	56	20	5
	EAZ 7	–	–	2	16	58	22	5
	EAZ 8	–	–	2	15	61	17	5
	EAZ 9	–	–	3	21	52	17	7

Skewness

The values of the skewness (SK_I) for the analyzed samples range between the maximum value of −0.31Φ, recorded in North Bara, and the minimum value of 0.2 Φ, found in East Abu Zabad. In the Jabra section 60% of the samples can be described as symmetrical, 33% are coarse skewed, and only one sample (7%) is fine skewed. In the North Bara section, 60% of the samples are considered symmetric, 33% are coarse skewed, and only 7% (one sample) is very coarse skewed. 78% of the samples from the West El Obeid section are symmetric and 22% are fine skewed. In East Abu Zabad, all samples are classified as fine skewed (Table 2; Fig. 7).

Kurtosis

The values of kurtosis (K_G) for all samples range from 0.64 to 1.89 Φ. The minimum and maximum values are recorded in Jabra and East Abu

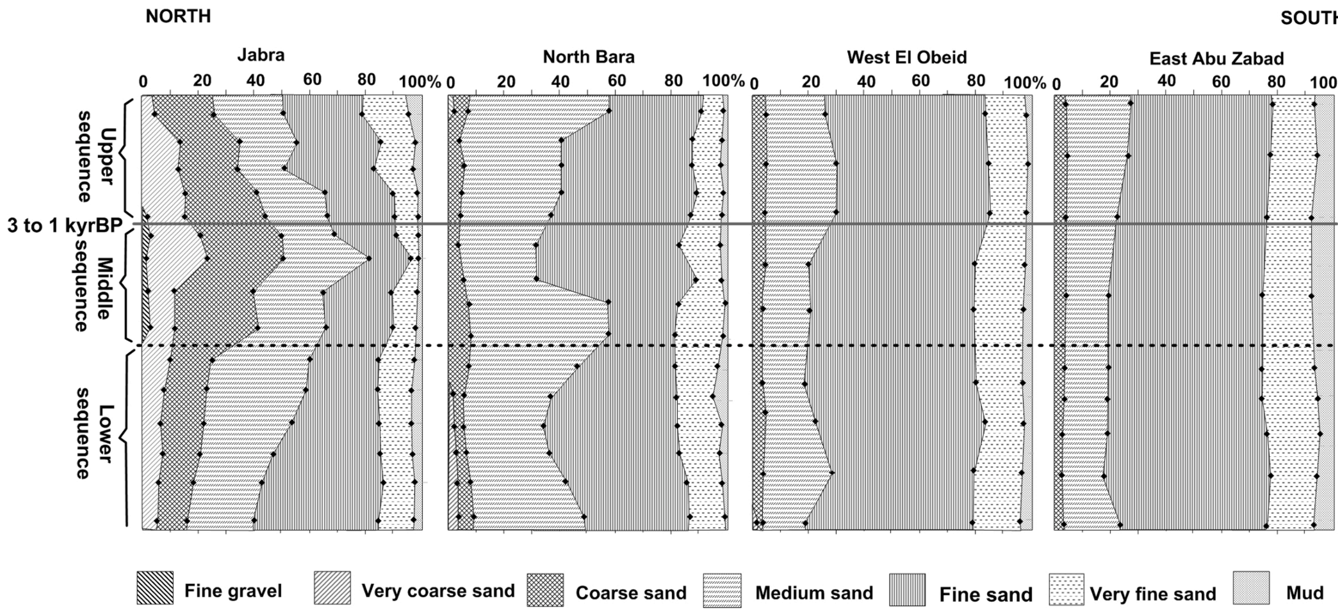

Fig. 6. Vertical evolution of grain size percentages. Datum is the discontinuity between the middle and upper sequence. The thicknesses of the sequences have been homogenized according to the thickest sections: North Bara for the upper sequence, Jabra for the middle sequence, and East Abu Zabad for the lower sequence.

Zabad, respectively. 73% of the samples from the Jabra section fall within the platykurtic range, 20% are mesokurtic and one sample (7%) is very platykurtic. In North Bara, 77% of the samples are leptokurtic and 33% are mesokurtic. In West El Obeid, 78% of samples fall within the leptokurtic range, one sample (11%) is very leptokurtic, and another one (11%) is mesokurtic. All samples in the East Abu Zabad section fall in the very leptokurtic range (Table 2; Fig. 7).

Log - probability curves

Forty-eight log-probability curves were constructed. The curves of each section are illustrated in one plot (Fig. 8). Thirty-five curves out of 48 show three straight line segments considered as three populations of grains transported by different processes. Thirteen curves (7 from Jabra and 6 from East Abu Zabad sections) show four straight line segments; thus, four populations are recognized, representing traction, suspension and two types of saltation transport processes.

The traction-saltation truncation points (TSTP) for all curves vary from ~1.5 to ~0.36 mm (−0.58 to 1.47Φ). The maximum and minimum TSTP are recorded in the Jabra and West El Obeid sections, respectively (Table 4). In the Jabra curves, the TSTP values of 53% of the samples fall within the very coarse sand, and 47% are within the coarse sand range. In the North Bara section, the TSTP values of 33% of the samples fall within the coarse sand, and 66% are within the medium sand range. In the West El Obeid section, TSTP values of 56% of the samples fall at the coarse-medium sand boundary, 33% in medium sand, and 11% (one sample) is in the coarse sand range. In the East Abu Zabad section, 67% of the samples have TSTP values that fall within the coarse sand range, and 33% of the samples plot within the medium sand range.

The saltation-suspension truncation points (SSTP) for all curves range from ~0.125 to ~0.056 mm (3.0 to 4.16Φ), recorded in the West El Obeid and Jabra sections, respectively (Table 4). In the Jabra section, 93% of the samples have SSTP values falling within the very fine sand range, while only 7% (one sample) fall within the very coarse silt. In the North Bara section, the SSTP values for all samples are within the very fine sand. However, some of them are exactly at the fine- to very fine sand boundary. For the West El Obeid and East Abu Zabad sections, the SSTP values for all samples fall within the very fine sand range.

Transport modes for all samples were calculated from Fig. 8 in terms of traction, saltation, and suspension populations, following Visher (1969). These calculated populations are expressed in percentages and size ranges (Table 4). The percentage of traction population for all samples ranges from ~1 to ~50%, recorded in the East Abu Zabad and Jabra sections, respectively. The percentage of saltation population (PSAP) ranges from 40 to ~95% for all samples, with both values recorded in the Jabra section. The percentage of suspension population for all samples varies from ~2 to ~20 % recorded in the Jabra and East Abu Zabad sections, respectively.

In term of size, grains transported by traction vary from ~2.2 to ~0.13 mm for all samples in the Jabra and West El Obeid sections, respectively. In the study area, grains transported by saltation fall within the size range of ~1.5 to ~0.059 mm for all samples. Both the coarsest and finest sizes are found in the Jabra section. In the study area, the maximum grain size transported as suspended sediment is ~0.121 mm, and is recorded in the Jabra section.

The calculated data in Table 4 were translated into grain populations evolution through time expressed in percentage variations (Fig. 9A), and into grain size variations for each section (Fig. 9B) to highlight both their vertical and lateral evolutions. Saltation dominates in all sections. In the Jabra section, however, the upper sequence is dominated by both traction and saltation populations as well as the top of the middle sequence. The percentage of traction population is generally low, except locally in the Jabra section, with a notable decrease to the south (Fig. 9A). The suspension population is greater in the southern sections than in the northern ones; it is variable in the northern sections (Jabra, North Bara) and decreases slightly upward in the southern sections.

The coarsest grain size transported by traction is recorded in the Jabra section, while the smallest size is recorded locally in the West El Obeid section. Both the coarsest and finest grain sizes transported by saltation are recorded in the Jabra section. However, the smallest grain size transported by saltation seems homogeneous in the lower sequence over the study area. The suspension population is coarsest in both the North Bara and West El Obeid sections (Fig. 9B).

In the lower and middle sequences of the Jabra section, the traction population is coarser than in the upper sequence; the traction-saltation and saltation-suspension contacts are regular in the lower sequence and irregular in the middle and upper sequences, the saltation population occupies a wide range. In North Bara, the traction population shows a slight fining-upward trend. Grain size of the saltation population is nearly constant, although a slight fining upward trend can be seen

Table 2
Summary of the calculated graphical statistics and their descriptions for the studied sections. Samples are numbered sequentially from top to bottom in each section. The Abbreviations in this table are explained in Table 3.

Section	Sample	Mean	Standard deviation		Skewness		Kurtosis	
			Value / phi	Description	Value /phi	Description	Value / phi	Description
JABRA	Jab 1	1.76	1.25	Ps	−0.21	Csk	0.87	Pk
	Jab 2	1.52	1.30	Ps	−0.08	Sy	0.79	Pk
	Jab 3	1.63	1.27	Ps	−0.22	Csk	0.64	Vpk
	Jab 4	1.39	1.28	Ps	−0.11	Csk	0.67	Pk
	Jab 5	1.34	1.22	Ps	0.06	Sy	0.68	Pk
	Jab 6	1.17	1.25	Ps	0.19	Fsk	0.75	Pk
	Jab 7	1.02	0.98	Ms	0.10	Sy	0.95	Pk
	Jab 8	1.44	1.20	Ps	−0.01	Sy	0.72	Pk
	Jab 9	1.40	1.27	Ps	−0.04	Sy	0.72	Pk
	Jab 10	1.72	1.15	Ps	0.04	Sy	0.80	Pk
	Jab 11	1.78	1.11	Ps	−0.09	Sy	0.84	Pk
	Jab 12	1.75	1.08	Ps	−0.05	Sy	0.83	Pk
	Jab 13	1.84	1.01	Ps	−0.05	Sy	0.95	Mk
	Jab 14	1.97	0.99	Ms	−0.27	Csk	1.00	Mk
	Jab15	2.03	0.96	Ms	−0.26	Csk	1.02	Mk
NORTH BARA	NB 1	2.22	0.83	Ms	−0.057	Sy	0.99	Lk
	NB 2	2.17	0.72	Ms	−0.071	Sy	1.24	Mk
	NB 3	2.17	0.82	Ms	−0.180	Csk	1.07	Lk
	NB 4	2.15	0.73	Ms	−0.135	Csk	1.22	Lk
	NB 5	2.12	0.73	Ms	−0.287	Vcsk	1.15	Lk
	NB 6	2.13	0.73	Ms	−0.312	Csk	1.21	Lk
	NB 7	2.28	0.72	Ms	−0.281	Csk	1.17	Lk
	NB 8	2.14	0.75	Ms	−0.160	Csk	1.19	Mk
	NB 9	1.94	0.78	Ms	−0.101	Sy	1.06	Lk
	NB 10	1.98	0.80	Ms	−0.091	Sy	1.13	Mk
	NB 11	2.18	0.97	Ms	0.098	Sy	1.31	Lk
	NB 12	2.19	0.84	Ms	−0.011	Sy	1.19	Lk
	NB 13	2.27	0.82	Ms	−0.007	Sy	1.24	Lk
	NB 14	2.25	0.84	Ms	0.067	Sy	1.27	Mk
	NB 15	2.03	0.90	Ms	0.086	Sy	1.11	Mk
WEST EL OBEID	WEO 1	2.35	0.66	MWs	−0.05	Sy	1.345	Lk
	WEO 2	2.27	0.60	MWs	−0.06	Sy	1.164	Lk
	WEO 3	2.31	0.64	MWs	0.04	Sy	1.328	Lk
	WEO 4	2.45	0.69	MWs	0.06	Sy	1.457	Lk
	WEO 5	2.42	0.64	MWs	0.12	Fsk	1.395	Lk
	WEO 6	2.33	0.70	MWs	0.09	Sy	1.438	Lk
	WEO 7	2.21	0.57	MWs	−0.07	Sy	1.048	Mk
	WEO 8	2.33	0.79	Ms	0.13	Fsk	1.542	Vlk
	WEO 9	2.42	0.79	Ms	0.05	Sy	1.496	Lk
EAST ABU ZABAD	EAZ 1	2.58	0.85	Ms	0.13	Fsk	1.62	Vlk
	EAZ 2	2.53	0.87	Ms	0.18	Fsk	1.57	Vlk
	EAZ 3	2.60	0.84	Ms	0.18	Fsk	1.69	Vlk
	EAZ 4	2.65	0.86	Ms	0.17	Fsk	1.89	Vlk
	EAZ 5	2.59	0.84	Ms	0.15	Fsk	1.67	Vlk
	EAZ 6	2.54	0.87	Ms	0.20	Fsk	1.82	Vlk
	EAZ 7	2.59	0.80	Ms	0.15	Fsk	1.88	Vlk
	EAZ 8	2.60	0.84	Ms	0.09	Sy	1.65	Vlk
	EAZ 9	2.58	0.87	Ms	0.19	Fsk	1.70	Vlk

Table 3
Abbreviation of the graphical statistic descriptions that shown in Table 2 and Fig. 7.

Standard deviation		Skewness		Kurtosis	
Description	Abbreviation	Description	Abbreviation	Description	Abbreviation
Very well sorted	*VWs*	Very fine skewed	*Vfsk*	Very platykurtic	*Vpk*
Well sorted	*Ws*	Fine skewed	*Fsk*	Platykurtic	*Pk*
Moderately sorted	*Ms*	Symmetrical	*Sy*	Mesokurtic	*Mk*
Poorly sorted	*Ps*	Coarse skewed	*Csk*	Leptokurtic	*Lk*
Very poorly sorted	*VPs*	Very coarse skewed	*Vcsk*	Very leptokurtic	*Vlk*
Extremely poorly sorted	*ExPs*			Extremely leptokurtic	*Exlk*

(Fig. 9B). In the latter section, the boundary between the saltation and suspension population shows very little grain size variation. The size range of the traction population in the West El Obeid and East Abu Zabad sections is narrow and stable over time. The grain size range of the saltation population shows a fining-upward trend. The contact between the saltation and suspension populations is fairly regular with a slight fining upward trend, and its grain size is generally less than 0.109 mm.

Interpretation

Energy of transport

Most of the continental siliciclastic sediments are transported by

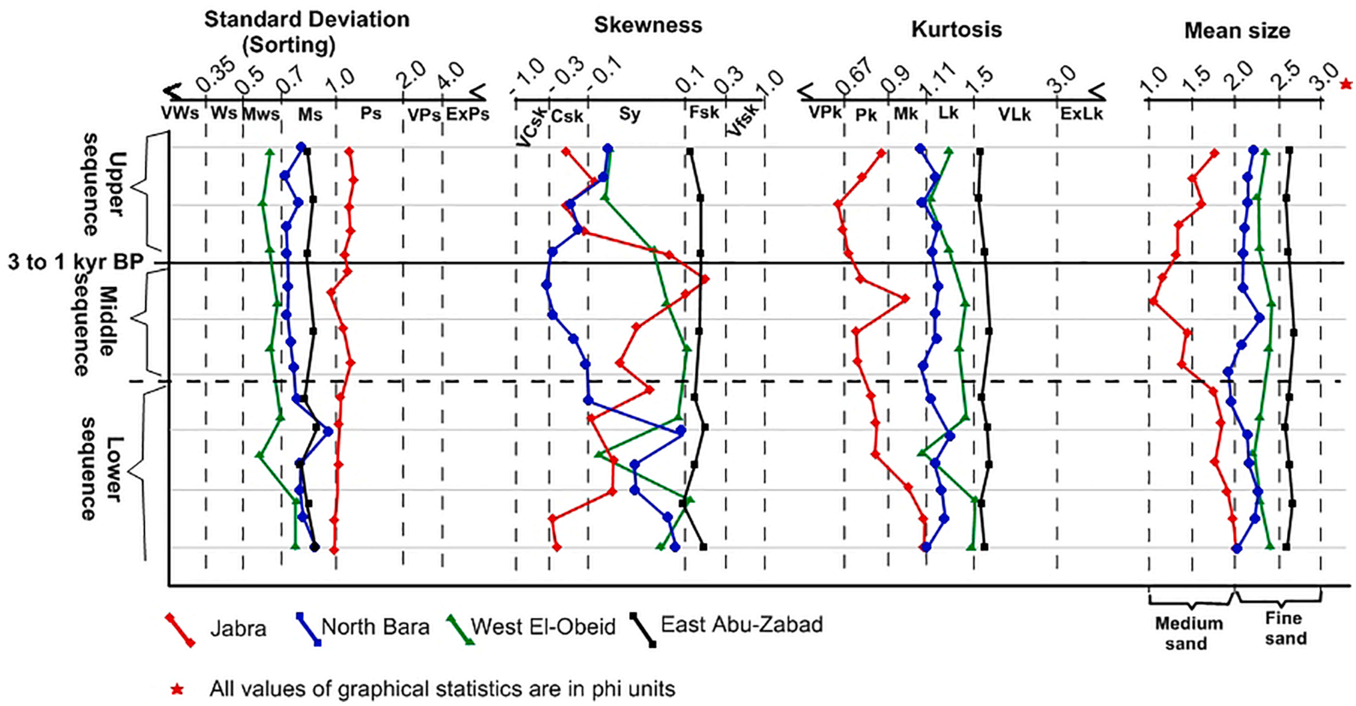

Fig. 7. Curves of pre- and post-hiatus graphical statistic plots for all sections. The curves for all sequences have been homogenized according to the thickest sections (North Bara for the upper sequence, Jabra for the middle sequence, and East Abu Zabad for the lower sequence). Abbreviations are explained in Table 3.

fluids (water) or winds (Boggs, 2006). The velocity, speed or strength of transportation factor have been expressed as energy by many sedimentologists (e.g. Folk and Ward, 1957; Visher, 1969; Tucker, 2003; Boggs, 2006; Nichols, 2009). Thus, we use the term "energy of transport" to express the strength of the transportation factor that allowed deposition of the Kordofan Sand. The transport energy can be inferred from the dispersion of the cumulative curves of the individual sections, the variation of grain size, and the graphical statistical intercorrelations. Based on these key parameters, we interpreted the energy of transport in terms of temporal and spatial evolutions.

Temporal evolution of energy

According to the grain size cumulative curves (Fig. 5), the samples from the Jabra section are widely scattered, reflecting a high variability in transport energy over time. In North Bara, the scatter of the curve is moderate, also reflecting variability in energy, while the curves from the other sites have a narrower scatter, indicating low variability in transport energy over time for West El Obeid, and energy stability for East Abu Zabad.

In all sequences, the grain size distribution in the Jabra section shows strong irregularities (Fig. 6), demonstrating a high variability of energy, with a notable upward increase from the lower to the middle sequence, as indicated by the presence of fine gravels in the middle sequence and the base of the upper sequence. The distribution is irregular in the North Bara section, indicating variable energy over time, while it is moderately regular in the West El Obeid section, indicating a moderately stable energy (with a notable upward decrease in energy around the lower-middle sequences boundary and in the middle sequence). The regular vertical distribution of grain size in the East Abu Zabad section indicates a stable energy of transport over time. Moreover, the samples from the northern part of the study area show a wide grain size distribution, indicating temporal variations in transport energy. Conversely, the samples from the southern areas show a narrow grain size distribution, indicating constant or low variability of transport energy during the same time-span.

The vertical homogeneity of the mean grain size in the East Abu Zabad, West El Obeid, and North Bara sections (Fig. 7), suggests uniform sedimentary processes, a common sedimentary origin, and a relative energy stability over time for all sequences. In contrast, the scatter of mean grain size values in Jabra not only indicates variable energy over time, but may also indicate multiple depositional mechanisms.

Skewness is a function of grain size and is geometrically independent of sorting (Folk and Ward, 1957). This means that if a sample is formed of very coarse to very fine sand, it can be described as coarsely skewed when the ratio of the very coarse sand is greater than the very fine sand; it can also be described as finely skewed if the amount of the very coarse sand exceeded the very fine sand (Folk and Ward, 1957). Therefore, it is difficult to use the skewness as a direct indicator of energy strength, but it can be used as an indicator of energy variation through time. The values of skewness (Fig. 7) are very heterogeneous in the northernmost Jabra section, heterogeneous in the North Bara section, homogeneous in the west El Obeid section, and very homogeneous in the southernmost East Abu Zabad section. This indicates that the temporal evolution of energy is highly variable in the Jabra section, variable in the North Bara section, stable in the west El Obeid section, and very stable in the East Abu Zabad section.

Spatial evolution of transport energy

The regular decrease in the mean grain size diagram from the northernmost Jabra section to the southernmost East Abu Zabad section (Fig. 7), indicates a gradual decrease in transport energy from North to South. The kurtosis curves evolve from North to South, from platykurtic to leptokurtic and very leptokurtic. This indicates a wide range of grain size and energy variability in the North, and a narrow range of grain size and a stable transport energy in the South.

In terms of grain size, the northernmost Jabra section shows poor sorting and abundant coarse grains (Fig. 6). Further South, the North Bara section is dominated by medium to fine sand, the West El Obeid section is dominated by fine sand, while the East Abu Zabad section is also dominated by fine sand with notable increases in very fine sand and mud contents. This distribution indicates a general southward fining trend, which in turn reflects a southward decrease in the energy of transport and deposition. The decrease in mean grain size from North to South (Fig. 7, right) supports this interpretation.

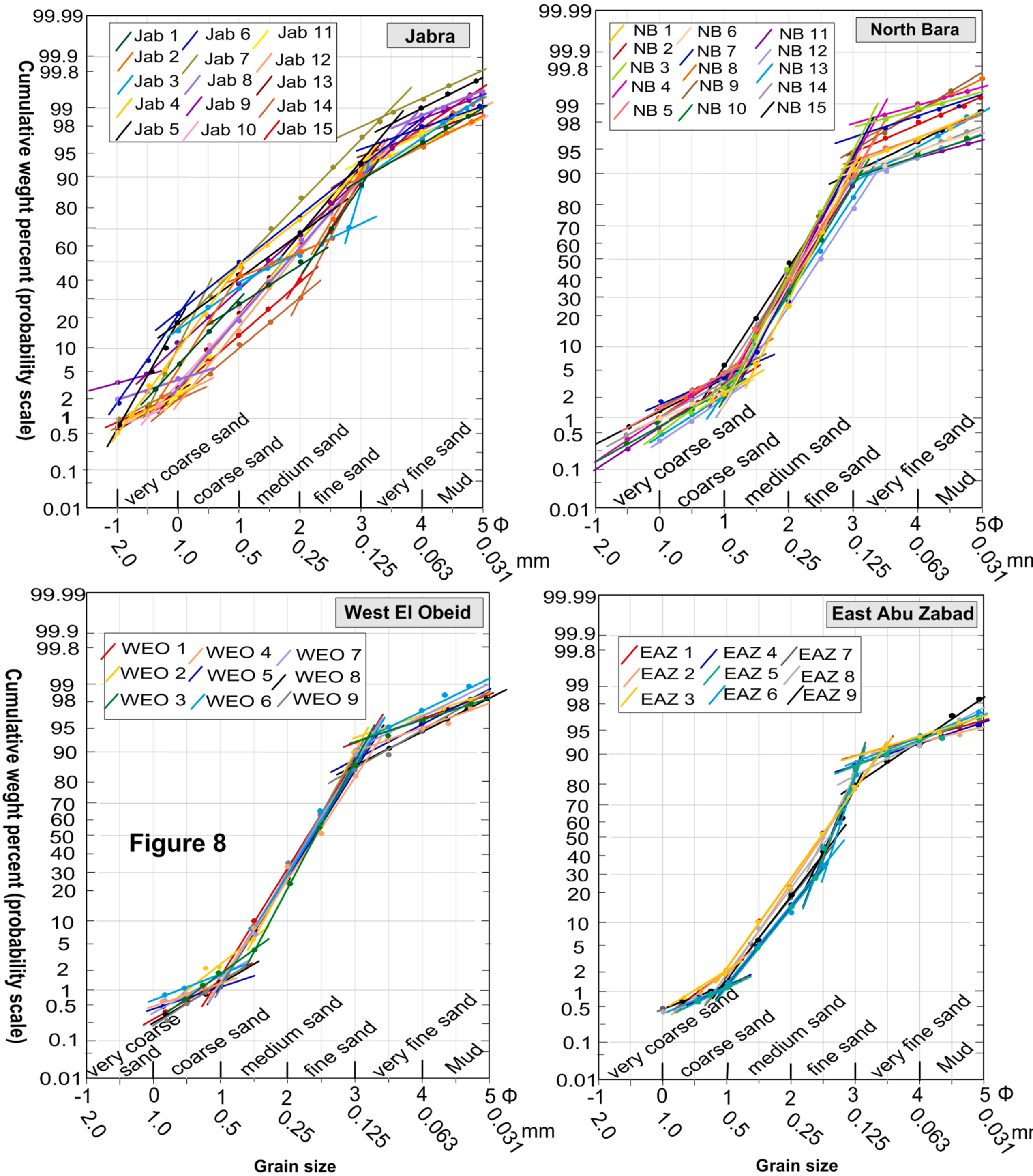

Fig. 8. Log-probability curves for all samples from the studied sections.

Fig. 10 shows that the maximum size driven by the traction mode picks up an average value of about 2.0, 1.3, 1.0, and 0.9 mm in the Jabra, North Bara, West El Obeid, and East Abu Zabad sections, respectively. This observation strongly supports the above interpretation of a generally southward decreasing energy.

Mode of transportation

The dominance of saltation population throughout the area (Fig. 9A) indicates the dominance of aeolian processes in the studied units (Visher, 1969). The high percentage of traction population in the upper sequence in Jabra (Fig. 9A) indicates that this unit was deposited under high energy, compared to the middle and lower sequences. However, the grain size range of the traction population of the upper sequence in the Jabra section is finer than in the middle and lower sequences (Fig. 9B), suggesting an opposite interpretation. These variations suggest that, either the energy was higher during deposition of the upper sequence than during that of the middle and lower sequences, or the sand of the middle and lower sequences was mixed with residual coarse grains.

In the North Bara, West El Obeid, and East Abu Zabad sections, stable transport modes with slightly fining upward trends (Fig. 9B) indicate that (1) depositional processes did not change over time, and (2) the

Table 4
Results of the transportation modes in the study area. TSTP is the traction-saltation truncation point and SSTP is the saltation-suspension truncation point. Samples are numbered sequentially from top to bottom in each section.

Section	Sample	TSTP (mm)	SSTP (mm)	Traction population		Saltation population		Suspension population	
				Percentage	Size range (mm)	Percentage	Size range (mm)	Percentage	Size range (mm)
JABRA	Jab 1	0.63	0.118	22	1.5–0.63	68	0.63–0.118	10	< 0.118
	Jab 2	0.5	0.121	41	1.35–0.5	50	0.5–0.121	10	< 0.121
	Jab 3	0.56	0.121	50	1.3–0.43	40	0.43–0.121	10	< 0.121
	Jab 4	0.5	0.111	44	2–0.5	49	0.5–0.111	7	< 0.111
	Jab 5	1.5	0.088	20	2.2–1.5	76	1.5–0.088	4	< 0.088
	Jab 6	1.0	0.081	23	2.2 – 1.0	75	1.0–0.081	2	< 0.081
	Jab 7	0.8	0.105	3	2.1–0.8	95	0.8–0.105	2	< 0.105
	Jab 8	0.86	0.081	3	2.1–0.86	94	0.86–0.081	3	< 0.081
	Jab 9	1.5	0.056	4	2.1–1.5	93	1.5–0.056	3	< 0.056
	Jab 10	1.25	0.111	2	2–1.25	90	1.25–0.111	8	< 0.111
	Jab 11	0.95	0.111	2.5	1.75–0.95	91.5	0.95–0.111	6	< 0.111
	Jab 12	1.0	0.111	2.5	1.75 – 1.0	92	1.0–0.111	5.5	< 0.111
	Jab 13	1.1	0.111	2.5	1.9–1.1	92	1.1–0.111	5.5	< 0.111
	Jab 14	1.15	0.111	2	2.1–1.15	92	1.15–0.111	6	< 0.111
	Jab15	1.25	0.111	2	2.15–1.25	92	1.25–0.111	6	< 0.111
NORTH BARA	NB 1	0.4	0.125	3	0.68–0.4	89	0.4–0.125	8	< 0.125
	NB 2	0.425	0.115	3	0.75–0.425	92	0.425–0.115	5	< 0.115
	NB 3	0.413	0.108	3.5	1.1–0.413	93.5	0.413–0.108	3	< 0.108
	NB 4	0.44	0.102	3.5	1.1–0.44	93.5	0.44–0.102	3	< 0.102
	NB 5	0.44	0.108	3.5	1.0–0.44	90.5	0.44–0.108	6	< 0.108
	NB 6	0.45	0.125	3	0.9–0.45	87	0.45–0.125	10	< 0.125
	NB 7	0.425	0.108	8	0.8–0.425	89	0.425–0.108	3	< 0.108
	NB 8	0.4	0.102	7	0.9–0.4	90	0.4–0.102	3	< 0.102
	NB 9	0.425	0.108	6	1.0–0.425	88	0.425–0.108	6	< 0.108
	NB 10	0.463	0.115	3	1.2–0.463	87	0.463–0.115	10	< 0.115
	NB 11	0.5	0.115	3	1.1–0.5	87	0.5–0.115	10	< 0.115
	NB 12	0.525	0.108	3	0.9–0.525	87	0.525–0.108	10	< 0.108
	NB 13	0.55	0.111	3	0.9–0.55	87	0.55–0.111	10	< 0.111
	NB 14	0.55	0.125	3	1.45–0.55	87	0.55–0.125	10	< 0.125
	NB 15	0.6	0.125	3	1.6–0.6	87	0.6–0.125	10	< 0.125
WEST EL OBEID	WEO 1	0.55	0.113	2	1.0–0.55	93	0.55–0.113	5	< 0.113
	WEO 2	0.36	0.121	7	0.88–0.36	89	0.36–0.121	4	< 0.121
	WEO 3	0.38	0.121	6	0.9–0.38	90	0.38–0.121	4	< 0.121
	WEO 4	0.43	0.121	5	0.93–0.43	89	0.43–0.121	6	< 0.121
	WEO 5	0.5	0.121	2	0.95–0.5	88	0.5–0.121	10	< 0.121
	WEO 6	0.5	0.118	2	0.95–0.5	87.5	0.5–0.118	10.5	< 0.118
	WEO 7	0.5	0.118	2	0.95–0.5	87	0.5–0.118	11	< 0.118
	WEO 8	0.5	0.125	2	0.95–0.5	86.5	0.5–0.125	11.5	< 0.125
	WEO 9	0.5	0.125	2	0.95–0.5	86	0.5–0.125	12	< 0.125
EAST ABU ZABAD	EAZ 1	0.48	0.063	2	0.9–0.48	90	0.48–0.063	8	< 0.063
	EAZ 2	0.45	0.074	2	0.9–0.45	89	0.45–0.074	9	< 0.074
	EAZ 3	0.49	0.095	2	0.8–0.49	88	0.49–0.095	10	< 0.095
	EAZ 4	0.5	0.115	1.5	0.75–0.5	85.5	0.5–0.115	13	< 0.115
	EAZ 5	0.52	0.118	1	0.9–0.52	85.5	0.52–0.118	13.5	< 0.118
	EAZ 6	0.58	0.118	1	1.05–0.58	85	0.58–0.118	14	< 0.118
	EAZ 7	0.58	0.118	1	1.1–0.58	84	0.58–0.118	15	< 0.118
	EAZ 8	0.58	0.118	1	0.95–0.58	82	0.58–0.118	17	< 0.118
	EAZ 9	0.55	0.118	1	0.9–0.55	79	0.55–0.118	20	< 0.118

transport energy did not evolve significantly over time, or was slightly decreasing through time.

The southward decrease in the percentages of the traction population (Fig. 9A), the southward increase in the percentages of the suspension population (Fig. 9A), and the southward fining trend of the traction population (Fig. 9B) all indicate that transport energy decreased southward during the deposition of the Kordofan Sand.

Discussion

The existence of the calcitic nodules resulting from pedogenesis in the lower and middle sequences might affect our results and interpretation. Such pedogenic calcitic features have been observed in Central Sudan, and are believed to have development during wetter climatic conditions (Dal Sasso, et al., 2018). Calcitic nodules in the Kordofan Sand were mostly developed above the water table as evidenced by their tubular morphology (Dawelbeit, 2018), which suggests that they formed through the replacement of organic material of roots by calcium carbonate (Alonso-Zarza et al., 2011). In addition, the presence of some biogenic features in the tubular calcrete suggests that it formed in the vadose zone (Arakel, 1996), where precipitation of carbonate usually occurs above the water table and within the sediment (Alonso-Zarza, 2003). This indicates that carbonate precipitated in the sediment after it has been deposited. Therefore, the presence of the calcitic nodules in the sampled sediments may affect the results of the grain size analysis. In order to avoid these nodules to be considered as individual grains, the calcareous nodules were removed as mentioned in section 3. For these reasons, we did not treat our samples with acid to remove the carbonate material. Since the calcitic nodules are concentrated in the lower sequence, their impact on the results should appear through the relative increase in the muddy fraction in the lower sequence. In fact, the results do not show such effects, as the percentages of the mud (silt and clay) shows approximately the same values along the sequences of each section (Table 1 and Fig. 6). Therefore, we assume that removing such nodules does not affect significantly the grain size distribution of the analyzed sediments. In more details, the muddy portion is greater in the upper sequence of the Jabra section than in the middle and lower sequence, although the upper sequence does not contain calcitic

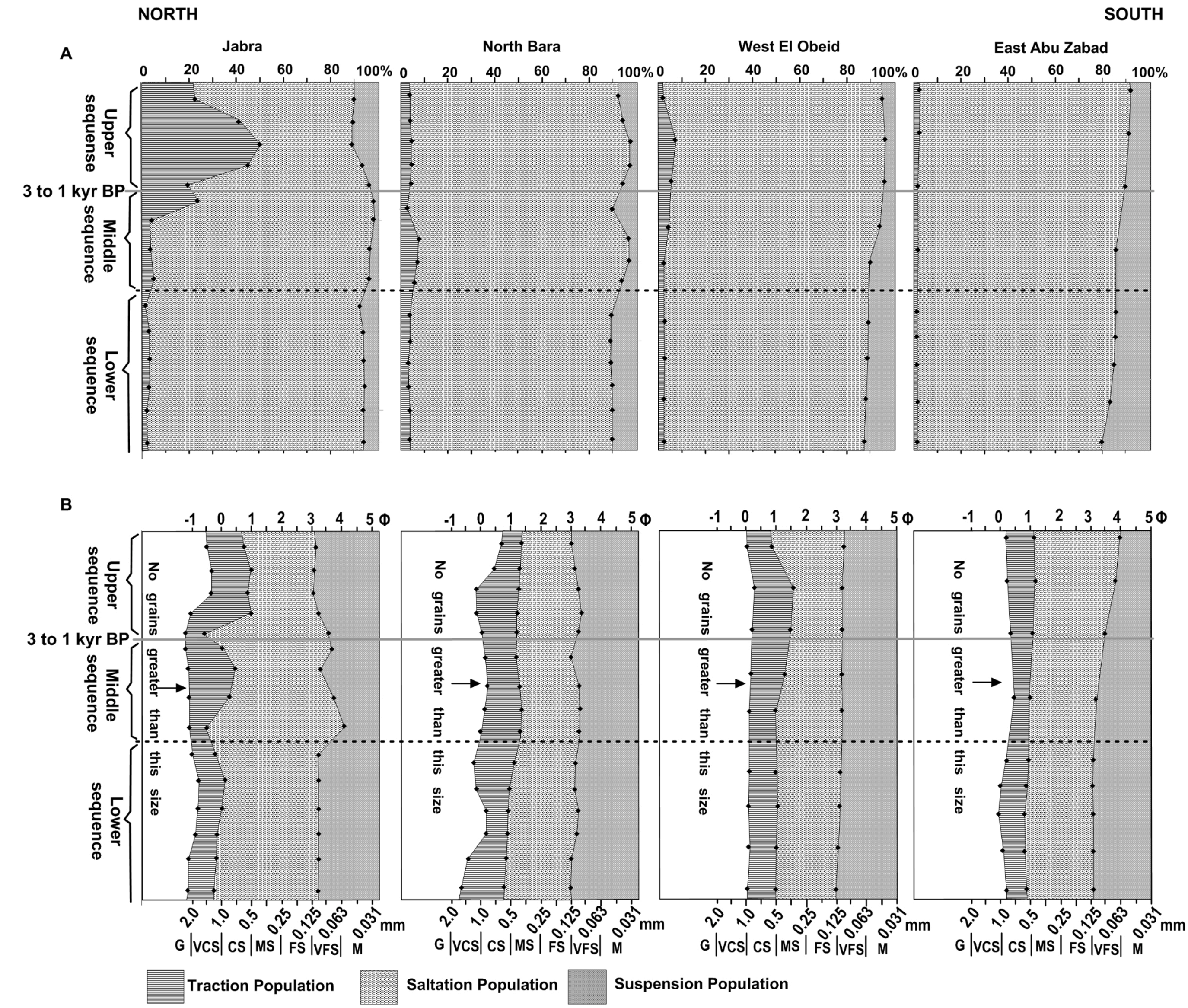

Fig. 9. Evolution of transport processes. (A) expressed in percentages, (B) expressed in grain size. Thicknesses have been homogenized according to the thickest sections (North Bara for the upper sequence, Jabra for the middle sequence, and East Abu Zabad for the lower sequence). In (B), the traction-saltation contact represents the traction-saltation truncation points (TSTP) or the coarse truncation points (CT) of the saltation mode as described by Visher (1969), while the saltation-suspension contact represents the saltation-suspension truncation points (SSTP) or the fine truncation points (FT) of the saltation mode as described by Visher (1969).

nodules. In the North Bara section, the muddy content is nearly constant throughout the three sequences, except in two samples in the lower and middle sequence. In the West El Obeid section, the slight upward decrease in the muddy content may represent a little effect of the calcitic nodules. In the East Abu Zabad section, the very homogeneous mud percentage throughout the sequences, indicates the absence of effects of calcitic nodule.

As reported in section 2.3, the Kordofan region, as much of the Saharan Desert, had been affected by the African Humid Period. Therefore, in addition to pedogenic features, these more humid conditions might have resulted in different post-depositional processes. The increase of rainfall likely favored the vegetation cover and consequently enhanced the pedogenesis, as discussed above. Vegetation might also have contributed in the stabilization of the sandy deposits, thus limiting aeolian transport. We are aware that this observation may influence our results regarding the second sequence. However, on one hand, the second sequence presents the coarsest grains in the Jabra section, showing that this influence was limited, and on the other hand, our work mainly focuses on mode of transport and the role of topography. The enhanced activity of organisms during wet periods might have also affected the grain size distribution through bioturbation processes, which might actively mix the sediment. We assume, however, that these processes did not affect significantly our result. As a matter of fact, no such mixing has been observed across the sequence boundaries, and sedimentary figures are commonly preserved (Dawelbeit et al., 2019a). Therefore, although our results may be viewed cautiously, we assume that they are representative.

When determining the depositional processes for different environments of ancient clastic rocks and sediments, Visher (1969) reported that the aeolian sediments are normally dominated by the saltation transportation mode. Therefore, the dominance of saltation in all studied sections (Table 4 and Fig. 9B), supports an aeolian origin of the Kordofan Sand. Vandenberghe (2013) wrote that grain-size analysis of aeolian sediments is a fairly valuable tool to distinguish different aeolian processes of transport and deposition, transport distance and origin in a particular sediment. This author pointed out that in purely aeolian

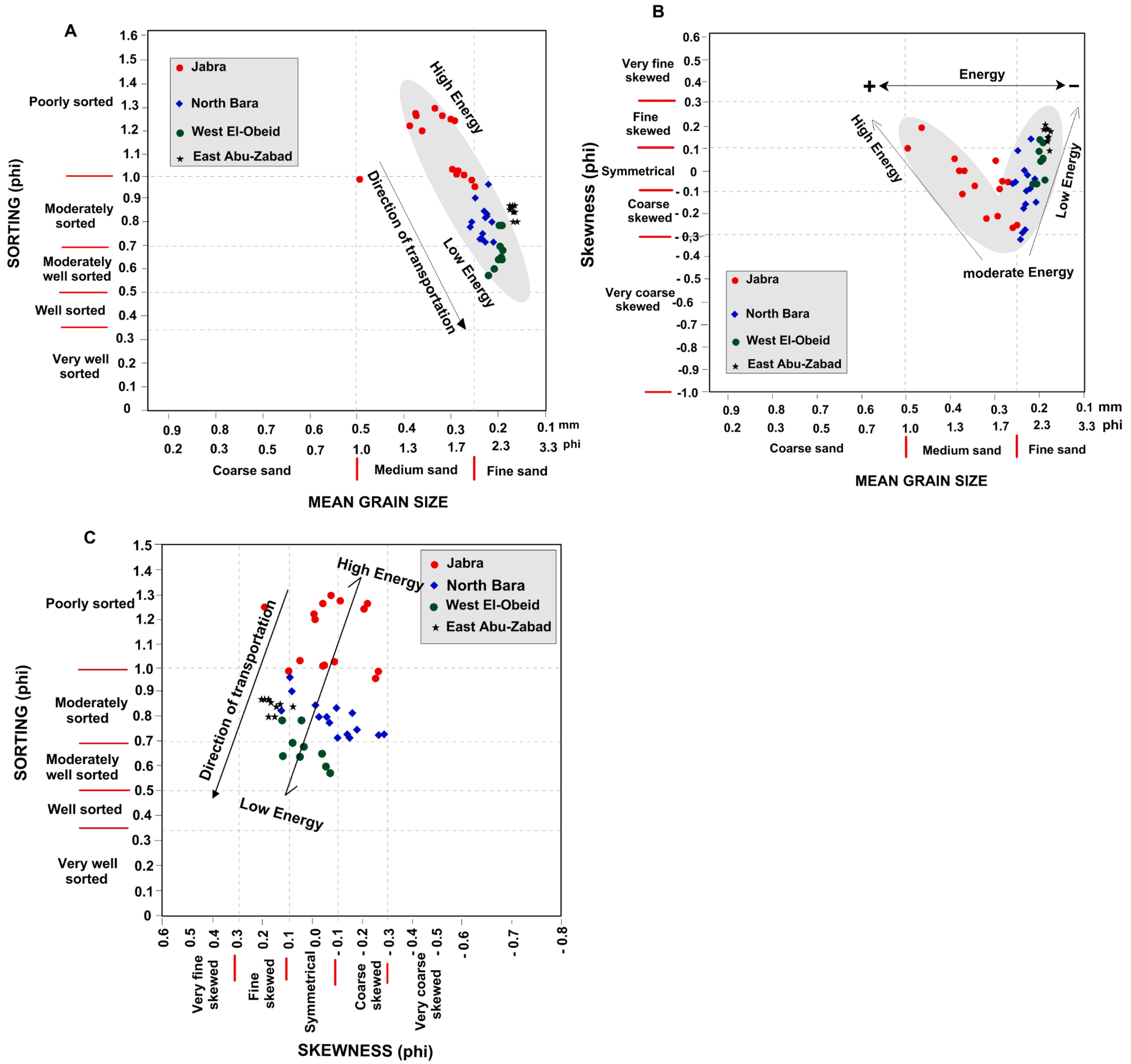

Fig. 10. Interrelation plots between the graphical statistics parameters indicating the transport energy. A: mean grain size *vs* sorting B: mean grain size *vs* skewness C: skewness *vs* sorting.

sediments, the fine sand to coarse silts of local origin are generally transported by saltation or in near-surface suspension, medium to coarse silts are transported in low suspension clouds as large dust, and fine to very fine silts and clays are transported over long distances in high suspension as small dust. However, these processes are controlled by many factors including provenance of the sediment, source area conditions, transport height above the surface, distance and direction of transport (Vandenberghe, 2013). In our studied sections, the sediments transported by saltation and suspension modes are coarser that those determined by Vandenberghe (Fig. 9B). Linking these observations with the observations by Visher (1969), we can conclude that the studied deposits are transported by aeolian processes from local origin that might be close to the Jabra section as suggested by Andrew (1948).

Among the various depositional environments, Visher (1969) reported that in fluvial environment, the coarse truncation points (CT) of the saltation mode and the fine truncation points (FT) of the saltation mode range from −1.5 to −1.0 Φ and from 2.75 to 3.5 Φ, respectively, while in well-sorted aeolian dune environment, CT and FT of the saltation mode range from 1.0 to 2.0 Φ and from 3.0 to 4.0 Φ, respectively. In the studied sediments, the CT in the Jabra section are range from −0.58 to 1.0 Φ and the FT are range from 3.05 to 4.16 Φ (Fig. 9B). Comparing these values with those determined by Visher, it appear that the coarse truncation points (CT) in the Jabra section are neither fall within CT range of fluvial nor aeolian environment; however, they fall between the fluvial and aeolian environments. This suggests that the sediments of the Jabra section have been reworked and experienced a weak degree of aeolian transport. On the other hand, the FT of saltation in the Jabra section have characteristics of both fluvial and aeolian sediments. In more details, the FT in the lower and upper sequences typically falls within the fluvial range and close to the FT of aeolian environment, while in the middle sequence and the base of the upper sequence, the FT fall mainly within the aeolian FT zone, with an upward inclination to the fluvial zone. These observations suggest that in the northern part of the study area, the sediments may have reworked fluvial deposits of paleo-rivers (fossil wadis) located west of the Jabra section (Fig. 2B). However, reworking due to aeolian activity is also considered. In the North Bara, West El Obeid, and East Abu Zabad sections, the CT points range from 0.74 to 1.32, 0.86 to 1.47, and from 0.79 to 1.15 Φ, respectively, while the FT points range from 3.0 to 3.29, 3.0 to 3.5, and 3.08 to 3.99 Φ, in the North Bara, West El Obeid and East Abu Zabad sections, respectively (Table 4 and Fig. 9B). Comparing these values with those determined by Visher (1969) and referring to Fig. 9B, we observe the following. (1) In the North Bara and East Abu Zabad sections, the CT for the upper and middle sequences fall within the aeolian range, while the CT for the lower sequence falls out of the aeolian range with clear upward inclination to the coarsest CT limit of the aeolian range of Visher (1969). (2) All CT values in the West El Obeid section fall within the CT aeolian field of Visher (1969), except one sample at the top of the section. (3) The FT points of the North Bara, West El Obeid, and East Abu Zabad sections are falling within the aeolian range of Visher (1969). Accordingly, the sediments of the North Bara, West El Obeid and East Abu Zabad sections are regarded as of typical aeolian environment. The small variation of the CT (in the lower sequence of these sections and those provided by Visher) can be explained in two ways. (1) Our studied sections are located in interdune and sand sheet environments (Fig. 2B), whereas Visher (1969) studied sediments of typical dune environment, and (2) the interdune and sand sheet environments are more likely to be affected by reworking processes, either aeolian or fluvial.

Bakhit and Ibrahim (1982) reported a tight relationship between the Kordofan Sand and the occurrence of the Nubian Sandstone Formation around the dunes and sand sheets. Supporting this suggestion, Whiteman (1971) reported the existence of outcrops of Nubian Sandstone Formation located north of our present study. However, because pre-Quaternary rocks are mostly covered by the Kordofan Sand (Fig. 2), their outcrops are of quite limited extension; moreover, the Nubian Sandstones are usually well lithified, and are usually coarser-grained than the studied deposits (McKee, 1963). Therefore, if the aeolian erosion of the Nubian Sandstones contributed to the origin of the studied deposits, its contribution was marginal.

On the other hand, Vandenberghe (2013) reported that aeolian sediments are often affected by post-depositional reworking. In the northern part of the studied area, large linear dunes grade southward into extensive sand sheets of Late Pleistocene age, which locally support still active transverse dunes and barchans (Fig. 2A). This shows that the Late Pleistocene large liner dunes are submitted to reworking until now. Consequently, we propose that the studied, mainly Holocene sand sequences were fed both by distal, fine-grained Saharan sands and by proximal, coarser-grained grains proceeding from the Late Pleistocene aeolian dunes. This may explain the presence of coarse grains (fine gravel to coarse sand) and the low degree of sorting observed in the northern sections. The increase in coarse grains in the northern sections, particularly grains transported by traction in the middle sequence and base of the upper sequence, suggests that this area experienced strong aeolian activity resulting in the removal of fine grains, which were transported further south as suspended sediments (Fig. 11). This can be correlated with the event of non-deposition between 3.3 and 1.1 kyr recorded in parts of Kordofan Region (Dawelbeit et al., 2019a). This hiatus, as well as the coarser grains of the upper sequence in the Jabra section and the aeolian erosion recorded in other sections can be correlated with (1) the increase in Saharan dust flux into the Atlantic between 5 and 0 kyr (Williams, 2014), (2) the desertification and

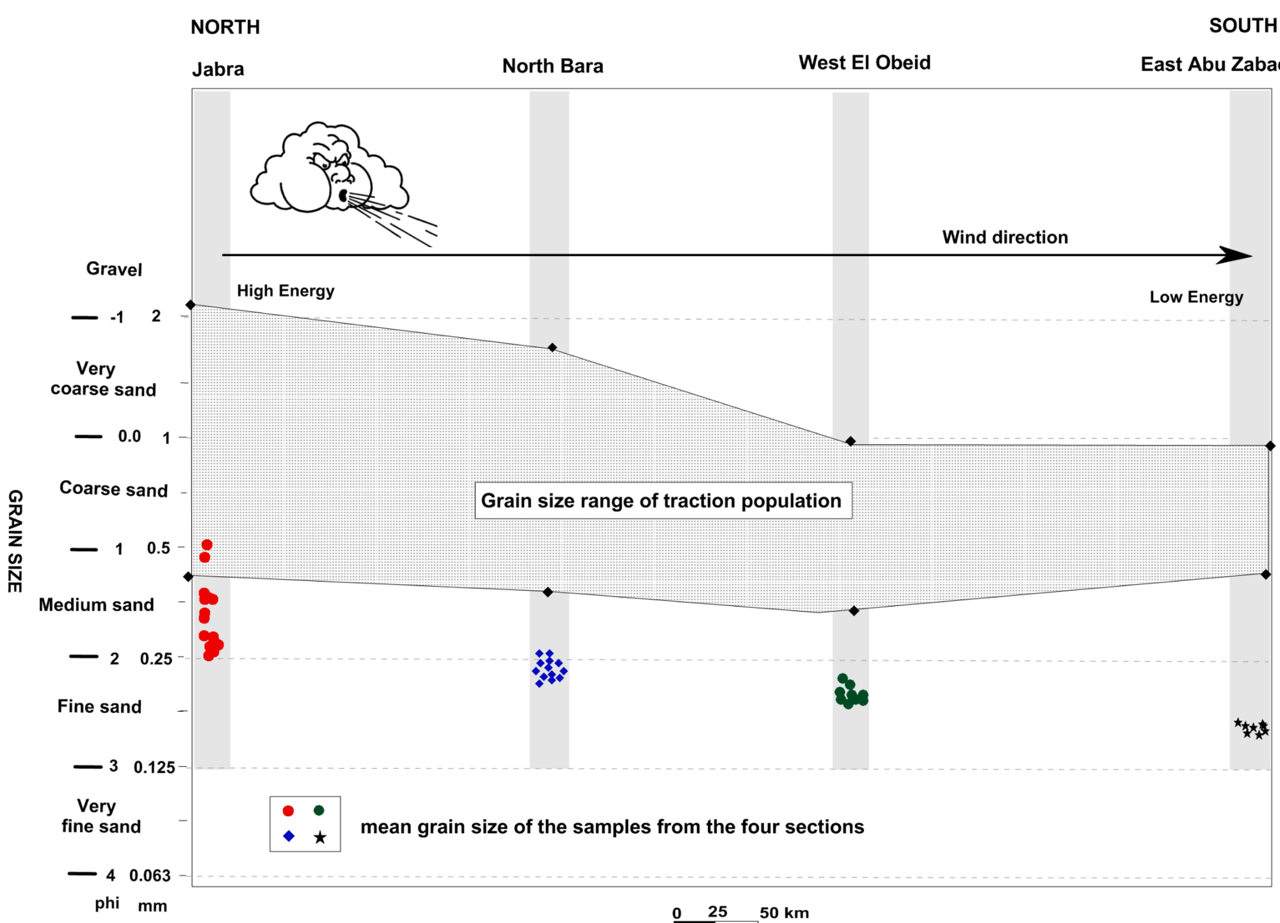

Fig. 11. Spatial mean grain-size and traction population size ranges, illustrating the North to South variation in transport energy and the wind direction.

aeolian deflation recorded during the middle and late Holocene in Egypt and northern Sudan (Nicoll, 2004), and (3) the wind regime established around 2.7 kyr B.P over the Sahara (Kröpelin et al., 2008).

To refine the above interpretation, we created interrelation plots between the graphical parameters. The plot of mean grain size *versus* sorting (Fig. 10A) shows a good linear relationship between the different sites and a clear trend from North to South. The shape of the mean grain size – sorting curve depends on the grain size range; it varies from the M-shaped, V-shaped or inverted V-shaped trend, and only one limb of V-shaped will develops if the range of grain size is wide, medium, and very small, respectively (Folk and Ward, 1957). The studied samples produced a linear trend, indicating that the grain size range is very small. However, one sample from the Jabra section, falls out of this linear trend, and it seems that relationship would have produce an inverted V-shaped trend if well-sorted, coarser-grained sediments were added in the northern part of the study area. Since the long distance of transportation results in well sorted sediments, and the grain size decreases whit the distance, the relationship in Fig. 10A, indicates a gradual decrease in energy from the Jabra to the West El Obeid section. The southernmost East Abu Zabad section is characterized by the finest mean grain size, and a less good sorting than the West El Obeid site.

The relationship between mean grain size and skewness does not show a linear relationship, but rather a "V" shape (Fig. 10B). Normally, in case of samples showing a bimodal grain size distribution or a wide grain size range, such relationship produces a sinusoidal curve with nearly equal numbers of positive-skewed and fine-skewed samples (Folk and Ward, 1957). Although the studied samples do not show a wide grain size range (Fig. 7), their mean size – skewness relationship, likely provide a V-shaped sinusoidal curve (Fig. 10B). On the other hand, the mean grain size is a positive function of energy, while the same skewness value can be found at both high and low energy. Therefore, the basal angle of the "V shaped curve" indicates the medium transport energy that led to the accumulation of these sediments, while the limbs of the "V" to the coarser and finer mean grain sizes indicate high and low energy, respectively.

The plot of sorting (standard deviation) *versus* skewness provides a linear relationship from Jabra to West El Obeid, supporting a decreasing transport energy from North to South (Fig. 10C). However, the East Abu Zabad sands are less sorted than the West El Obeid samples, and also less than part of those from North Bara. This peculiarity of the East Abu Zabad section can be attributed to a sudden drop in energy due to its geographical location in the lee side of a topographic crest, which protects this site from high energy dominant winds (Fig. 2C). This drop in energy would result in the rapid deposition of suspended sediment with less efficient sorting.

Nottebaum et al. (2014) suggested that topography may play an important role in terms of sediment supply and availability along aeolian transport pathways. This hypothesis may provide an explanation for (1) the sudden drop in energy and the relatively less sorted sediments seen in East Abu Zabad section, which is located on the lee side of a topographic crest (Fig. 2C), and (2) the availability of coarse residual particles to the North with the southward decrease in grain size along the transport pathway.

Conclusions

The Holocene Kordofan Sand comprises a lower, pedogenized, yellow to pale grey sand sequence, a middle, mildly pedogenized pale yellow to light brown sand sequence, and an upper, little or non-pedogenized red sand sequence. Locally, the lower and middle sequences are separated by palustrine and lacustrine carbonates. All sequences show vertical and geographic variations in grain size distribution. The vertical grain size variations reflect a variable and high energy of transport over time in the northern area, while in the South, the energy was low and stable over time. The spatial grain size distribution shows generally coarser size in the North and a gradual decrease towards the South, where very fine-grained sand predominates. Such geographical variation suggests that the Kordofan sand was transported from North to South. The dominance of the saltation mode of transport in all areas suggests a common aeolian depositional environment for all sequences. Finally, the topography of the northern part of the study area, characterized by a gently north-dipping slope, opposite to wind direction, strongly contributed to the erosion of fine sediments, which were probably deposited in the southern part of the study area, which is located in the lee side of the central plateau, and thus sheltered from the prevailing winds. The studied sediments have the characteristics of both distal and proximal source. This is evidenced by their low sorting degree, the presence of coarse grains, and the still active transverse dunes and barchans in the North, which indicate that the Late Pleistocene part of the Kordofan Sandstone is submitted to reworking until now. Consequently, the mainly Holocene sand sequences were fed both by distal, fine-grained Saharan sands and by proximal, coarser-grained sediments proceeding from the Late Pleistocene aeolian dunes of the Kordofan region.

Declaration of Competing Interest

The authors declare that they have no known competing financial interests or personal relationships that could have appeared to influence the work reported in this paper.

Acknowledgements

This study was conducted thanks to a doctoral grant provided to A. Dawelbeit by the Sudanese Government. The field trips and analyses were funded by the French-Sudanese collaborative projects "Napata" n° 38408UF and 38730A, by the ISTerre laboratory (Grenoble, France), and by the IRD institution (Marseille, France). The authors would like to thank the French Embassy in Khartoum and the Ministry of Higher Education and Scientific Research of Sudan for their support, and the Department of Geology of the University of Kordofan (El Obeid) for the free sieving of samples. Special thanks to Mr. Badr-Eddeen En Nour (Univ. of Kordofan) for his help in sampling during the field work and for conducting the grain size analysis. Our thanks extend to the reviewers and editor, who made thoughtful comments and suggestions that helped a lot in presenting this paper in its current form.

References

Abdel Galil, M.Y., 2008. Geology and Mineralization related to anorogenic igneous complex of Northern Nuba Mountains and Northern Kordofan, Sudan. Al Neelain University, Sudan. PhD Thesis.
Abdu, A., 1976. The Crescentic dunes of northern Sudan. East Afr. Geogr. Rev. 14, 61–71.
Alonso-Zarza, A.M., 2003. Palaeoenvironmental significance of palustrine carbonates and calcretes in the geological record. Earth-Sci. Rev. 60 (3-4), 261–298.
Alonso-Zarza, A.M., Genise, J.F., Verde, M., 2011. Sedimentology, diagenesis and ichnology of Cretaceous and Palaeogene calcretes and palustrine carbonates from Uruguay. Sed. Geol. 236 (1-2), 45–61.
Andrew, G., 1948. Geology of the Sudan. In: Tothill (Ed.), Agriculture in the Sudan. Oxford Univ Press, pp. 84–128.
Arakel, A.V., 1996. Quaternary vadose Calcretes revisited. J. Australian Geol. Geophys. 16, 223–229.
Bagnold, R.A., 1941. Physics of blown sand and desert dunes. In: Visher, G., 1969. Grain size distributions and depositional processes. J. Sedim. Petrol., 39, 1074-1106.
Bakhit, A., Ibrahim, F.N., 1982. Geomorphological aspects of the process of desertification in Western Sudan. GeoJournal 6 (1), 19–24.
Boggs, S., 2006. Principles of Sedimentology and Stratigraphy, fourth ed. Prentice-Hall, New Jersey, p. 662.
Costantini, E.A.C., 2018. Paleosols and pedostratigraphy. Appl. Soil Ecol. 123, 597–600.
Costantini, E.A.C., Priori, S., 2007. Pedogenesis of plinthite during early Pliocene in the Mediterranean environment – case study of a buried paleosol at Podere Renieri, central Italy. Catena 71 (3), 425–443.
Dal Sasso, G., Zerboni, A., Maritan, L., Angelini, I., Compostella, C., Usai, D., Gilberto Artioli, D., 2018. Radiocarbon dating reveals the timing of formation development of pedogenic calcium carbonate concretions in Central Sudan during the Holocene. Geochim. Cosmochim. Acta 238, 16–35.
Dawelbeit, A., 2018. Late Quaternary sedimentary and paleoclimatic evolution of Kordofan, Sudan. Université Grenoble Alpes. PhD thesis, https://www.theses.fr/2018GREAU022.

Dawelbeit, A., Jaillard, E., Eisawi, A., 2019a. Sedimentary and paleobiological records of the Holocene climate evolution in Kordofan region, Sudan. J. Afr. Earth Sci. 160, 1–15.
Dawelbeit, A., Jaillard, E., Eisawi, A., 2019b. Paleoclimate evolution of the Kordofan Region (Sudan), during the last 13 ka. In: Zhang, Z., Khélifi, N., Mezghani, A., Heggy, E. (Eds.), Patterns and Mechanisms of Climate, Paleoclimate and Paleoenvironmental Changes from Low-Latitude Regions. Springer, Berlin, Heidelberg, pp. 25–28.
Edmond, J.M., 1942. The distribution of the Kordofan Sands "Anglo-Egyptian Sudan". Geol Magazine. 79, 18–30.
Egerer, S., Claussen, M., Reick, C., Stanelle, T., 2017. Could gradual changes in Holocene Saharan landscape have caused the observed abrupt shift in North Atlantic dust deposition? Earth Planet. Sci. Lett. 473, 104–112.
El Shafie, A.A.I., Elsayed Zeinelabdein, K.A., Eisawi, A.A.M., 2013. Paleoclimatic evolution of central Sudan during the Late Miocene to Pleistocene. Arab J Geosci 6 (5), 1517–1525. https://doi.org/10.1007/s12517-011-0435-z.
Elmansour, A.A., 2017. Assessment of the Groundwater of En Nuhud Basin, West Kordofan State-Sudan. University of West Kordofan, p. 178. Doctoral thesis.
Elmansour, A.A., Omer, O.A., 2017. Crustal architecture, geodynamics and evolution of En Nuhud basin area, Kordofan region, Sudan. Int. J. Adv. Geosci. 5, 121–132.
Folk, R.L., 1971. Longitudinal dunes of the northwestern edge of the Simpson Desert, northern Territory, Australia, 1. Geomorphology and grain size relationships. Sedimentology 16 (1-2), 5–54.
Folk, R.L., Ward, W.C., 1957. Brazos River Bar: a study in the significance of grain size parameters. J. Sedim. Petrol. 27, 3–26.
Gasse, F., Chalié, F., Vincens, A., Williams, M.A.J., Williamson, D., 2008. Climatic patterns in equatorial and southern Africa from 30,000 to 10,000 years ago reconstructed from terrestrial and near-shore proxy data. Quat. Sci. Rev. 27 (25-26), 2316–2340.
Gatto, M.C., Zerboni, A., 2015. Holocene Supra-regional environmental changes as trigger for major socio-cultural processes in Northeastern Africa and the Sahara. Afr. Archaeol. Rev. 32 (2), 301–333.
Gierz, P., Werner, M., Lohmann, G., 2017. Simulating climate and stable water isotopes during the Last Interglacial using a coupled climate-isotope model. J. Adv. Model. Earth Syst. 9 (5), 2027–2045. https://doi.org/10.1002/2017MS001056.
Ginaya, M.A., 2011. Updating of Groundwater Conditions of Ennahud Basin - North Kordofan, Sudan. PhD Thesis, Institute for Energy and Earth Sciences, Sudan. 183 p.
Grabham, G., 1935. In: The Anglo-Egyptian Sudan from Within, pp. 257–281. London.
Kröpelin, S., Verschuren, D., Lézine, A.-M., Eggermont, H., Cocquyt, C., Francus, P., Cazet, J.-P., Fagot, M., Rumes, B., Russell, J.M., Darius, F., Conley, D.J., Schuster, M., von Suchodoletz, H., Engstrom, D.R., 2008. Climate-driven ecosystem succession in the Sahara: the past 6000 years. Science 320 (5877), 765–768.
Liu, B., Qu, J., Ning, D., Gao, Y., Zu, R., An, Z., 2014. Grain-size study of aeolian sediments found east of Kumtagh Desert. Aeolian Res. 13, 1–6.
McGee, D., deMenocal, P.B., Winckler, G., Stuut, J.B.W., Bradtmiller, L.I., 2013. The magnitude, timing and abruptness of changes in North African dust deposition over the last 20,000 yr. Earth Planet. Sci. Lett. 371-372, 163–176.
McKee, E.D., 1963. Origin of the Nubian and similar sandstones. Geol. Rundsch. 52 (2), 551–587.
McLaren, P., Bowles, D., 1985. The effects of sediment transport on grain-size distributions. J Sedim Petrol. 55, 457–470.
Nichols, G., 2009. Sedimentology and Stratigraphy, second ed. John Wiley & Sons Ltd., UK, p. 419p.
Nicholson, S.E., Flohn, H., 1980. African Environmental and Climatic changes and the general atmospheric circulation in Late Pleistocene and Holocene. Clim. Change 2 (4), 313–348.
Nicoll, K., 2004. Recent environmental change and prehistoric human activity in Egypt and Northern Sudan. Quatern. Sci. Rev. 23 (5-6), 561–580.
Nottebaum, V., Lehmkuhl, F., Stauch, G., Hartmann, K., Wünnemann, B., Schimpf, S., Lu, H., 2014. Regional grain size variations in aeolian sediments along the transition between Tibetan highlands and north-western Chinese deserts – the influence of geomorphological settings on aeolian transport pathways. Earth Surf. Process. Landforms. 39 (14), 1960–1978.
Rajganapathi, V.C., Jitheshkumar, N., Sundararajan, M., Bhat, K.H., Velusamy, S., 2013. Grain-size analysis and characterization of sedimentary environment along Tiruchendur coast, Tamilnadu. India. Arab J. Geosci. 6, 4717–4728.
Revel, M., Ducassou, E., Grousset, F.E., Bernasconi, S.M., Migeon, S., Revillon, S., Mascle, J., Murat, A., Zaragosi, S., Bosch, D., 2010. 100,000 years African monsoon variability recorded in sediments of the Nile margin. Quat. Sci. Rev. 29, 1342–1362.
Rodis, H.G., Hassan, A., Wahadan, L., 1968. Groundwater Geology of Kordofan Province-Sudan, Contribution to the hydrology of Africa and Mediterranean Region. United State government printing office. Washington.
Ruxton, B.P., Berry, L., 1978. Clay plain and geomorphic history of the Central Sudan - a review. Catena. 5, 251–283.
Schrank, E., 1994. Nonmarine Cretaceous palynology of northern Kordofan, Sudan, with notes on fossil Salviniales (water ferns). Geol. Rundsch 83, 773–786.
Schwarz, T., 1994. Ferricrete formation and relief inversion: an example from Central Sudan. Catena 21 (2-3), 257–268. Sedimentology. 61, 225–267. Elsevier, Amsterdam.
Swezey, C., 2001. Eolian sediment responses to late Quaternary climate changes: temporal and spatial patterns in the Sahara. Palaeog. Palaeoclimat, Palaeoecol. 167 (1-2), 119–155.
Tierney, J.E., Russell, J.M., Sinninghe Damsté, J.S., Huang, Y., Verschuren, D., 2011. Late Quaternary behavior of the East African monsoon and the importance of the Congo Air Boundary. Quatern Sci Reviews. 30 (7-8), 798–807.
Tierney, J.E., deMenocal, P.B., Zander, P.D., 2017. A climatic context for the out-of-Africa migration. Geology 45 (11), 1023–1026.
Tucker, M.E., 2003. Sedimentary Rocks in the Field, third ed. John Wiley & Sons Ltd., Englad, p. 234.
Udden, J.A., 1914. Mechanical composition of clastic sediments. Bull. Geol. Soc. Amer. XXV 25 (1), 655–744.
Vail, J.R., 1978. Outline of the geology and mineral deposits of the Democratic Republic of the Sudan and adjacent areas. Overseas Geol. Mineral Resourc. 49, 66 pp.
Vandenberghe, J., 2013. Grain size of fine-grained windblown sediment: A powerful proxy for process identification. Earth-Sci. Rev. 121, 18–30.
Vandenberghe, J., Sun, Y., Wang, X., Abels, H.A., Liu, X., 2018. Grain-size characterization of reworked fine-grained aeolian deposits. Earth-Sci. Rev. 177, 43–52.
Visher, G., 1969. Grain size distributions and depositional processes. J. Sedim. Petrol. 39, 1074–1106.
Wentworth, C.K., 1922. A scale of grade and class terms for clastic sediments. J. Geol. 30 (5), 377–392.
Whiteman, A.J., 1971. The Geology of the Sudan Republic. Oxford University Press, London, p. 303.
Williams, M.A.J., 2009. Late Pleistocene and Holocene environments in the Nile basin. Glob. Planet. Chang. 69 (1-2), 1–15.
Williams, M.A.J., 2014. Climate Change in Deserts (past, present and future). Cambridge University Press, New York, p. 629.
Williams, M.A.J., Adamson, D., Cock, B., McEvedy, R., 2000. Late Quaternary environments in the White Nile region, Sudan. Global Planet Change. 26, 305–316.
Williams, M., Talbot, M., Aharon, P., Abdl Salaam, Y., Williams, F., Inge Brendeland, K., 2006. Abrupt return of the summer monsoon 15,000 years ago: new supporting evidence from the lower White Nile valley and Lake Albert. Quat. Sci. Rev. 25 (19-20), 2651–2665.
Woodward, J.C., Macklin, M.G., Michael, D., Krom, D., Williams, M.A.J., 2007. The Nile: Evolution, Quaternary River Environments and Material Fluxes, in: Large Rivers: Geomorphology and Management. 261-292. John Wiley and Sons Ltd.
Zerboni, A., Trombino, L., Frigerio, C., Livio, F., Berlusconi, A., Michetti, A.M., Rodnight, H., Spötl, C., 2015. The loess-paleosol sequence at Monte Netto: a record of climate change in the Upper Pleistocene of the central Po Plain, northern Italy. J. Soils Sediments 15 (6), 1329–1350.
Zhu, B., Yu, J., 2014. Aeolian sorting processes in the Ejina desert basin (China) and their response to depositional environment. Aeolian Res. 12, 111–120.
Zielhofer, C., von Suchodoletz, H., Fletcher, W.J., Schneider, B., Dietze, E., Schlegel, M., Schepanski, K., Weninger, B., Mischke, S., Mikdad, A., 2017. Millennial-scale fluctuations in Saharan dust supply across the decline of the African Humid Period. Quat. Sci. Rev. 171, 119–135.